

**TECHNICAL REPORT
NATICK/TR-10/018**



AD _____

DEVELOPMENT OF AN ADVANCED FLAMELESS COMBUSTION HEAT SOURCE UTILIZING HEAVY FUELS

**by
Clifford G. Welles**

**Catalytic Devices International, LLC
Pleasanton, CA 94588**

July 2010

**Final Report
February 2006 – June 2008**

Approved for public release; distribution is unlimited.

**Prepared for
U.S. Army Natick Soldier Research, Development and Engineering Center
Natick, Massachusetts 01760-5018**

UNCLASSIFIED

DISCLAIMERS

The findings contained in this report are not to be construed as an official Department of the Army position unless so designated by other authorized documents.

Citation of trade names in this report does not constitute an official endorsement or approval of the use of such items.

DESTRUCTION NOTICE

For Classified Documents:

Follow the procedures in DoD 5200.22-M, Industrial Security Manual, Section II-19 or DoD 5200.1-R, Information Security Program Regulation, Chapter IX.

For Unclassified/Limited Distribution Documents:

Destroy by any method that prevents disclosure of contents or reconstruction of the document.

REPORT DOCUMENTATION PAGE					Form Approved OMB No. 0704-0188	
Public reporting burden for this collection of information is estimated to average 1 hour per response, including the time for reviewing instructions, searching existing data sources, gathering and maintaining the data needed, and completing and reviewing this collection of information. Send comments regarding this burden estimate or any other aspect of this collection of information, including suggestions for reducing this burden to Department of Defense, Washington Headquarters Services, Directorate for Information Operations and Reports (0704-0188), 1215 Jefferson Davis Highway, Suite 1204, Arlington, VA 22202-4302. Respondents should be aware that notwithstanding any other provision of law, no person shall be subject to any penalty for failing to comply with a collection of information if it does not display a currently valid OMB control number.						
PLEASE DO NOT RETURN YOUR FORM TO THE ABOVE ADDRESS.						
1. REPORT DATE (DD-MM-YYYY) 07-07-2010		2. REPORT TYPE Final		3. DATES COVERED (From - To) February 2006 - June 2008		
4. TITLE AND SUBTITLE DEVELOPMENT OF AN ADVANCED FLAMELESS COMBUSTION HEAT SOURCE UTILIZING HEAVY FUELS				5a. CONTRACT NUMBER W911QY-05-C-0064		
				5b. GRANT NUMBER		
				5c. PROGRAM ELEMENT NUMBER 622786		
6. AUTHOR(S) Clifford G. Welles				5d. PROJECT NUMBER		
				5e. TASK NUMBER		
				5f. WORK UNIT NUMBER		
7. PERFORMING ORGANIZATION NAME(S) AND ADDRESS(ES) Catalytic Devices International, LLC 7063-E Commerce Circle Pleasanton, CA 94588				8. PERFORMING ORGANIZATION REPORT NUMBER		
9. SPONSORING / MONITORING AGENCY NAME(S) AND ADDRESS(ES) U.S. Army Natick Soldier Research, Development and Engineering Center ATTN: RDNS-CFE (A. Schmidt) Kansas Street, Natick, MA 01760-5018				10. SPONSOR/MONITOR'S ACRONYM(S)		
				11. SPONSOR/MONITOR'S REPORT NUMBER(S) NATICK/TR-10/018		
12. DISTRIBUTION / AVAILABILITY STATEMENT Approved for public release; distribution is unlimited.						
13. SUPPLEMENTARY NOTES						
14. ABSTRACT <i>Report developed under Broad Agency Announcement contract.</i> Advance Flameless Catalytic Combustion Technology (AFCT) is a collection of innovative, proprietary techniques and processes that have demonstrated effectiveness in overcoming problems associated with stabilizing captive flameless heat generation. CDI's unique success in achieving stabilization in captive combustion for light fuels such as methanol, ethanol and butane was extended to include heavy fuels such as JP-8 and diesel and also to increase the thermal power output to include near kilowatt levels. A complete re-design of the critical subsystem components was required. The results were then utilized to construct a catalytic Flow-Through Water Heater demonstration prototype unit, intended as a portable accessory for the soldier personal hydration pack.						
15. SUBJECT TERMS						
FUELS	CATALYSIS	FLAMELESS	WATER HEATER			
WATER	JET-A FUEL	PROTOTYPES	SYSTEM DESIGN			
HEATING	PORTABLE	COMBUSTION	FUEL CONSUMPTION			
JP-8 FUELS	OXIDATION	HEAVY FUELS	TRANSPORT PROPERTIES			
KEROSENE	HYDRATION	VAPORIZATION	BAA(BROAD AGENCY ANNOUNCEMENT)			
16. SECURITY CLASSIFICATION OF:			17. LIMITATION OF ABSTRACT	18. NUMBER OF PAGES	19a. NAME OF RESPONSIBLE PERSON	
a. REPORT	b. ABSTRACT	c. THIS PAGE			Alex Schmidt	
U	U	U	SAR	80	19b. TELEPHONE NUMBER (include area code) (508) 233-6042	

This page intentionally left blank

UNCLASSIFIED

Table of Contents

List of Figures.....	iv
List of Tables	v
Preface.....	vi
1. Summary.....	1
2. Introduction.....	2
3. Milestones and Timeline.....	4
3.1 Overview of Significant Project Milestones	4
3.2 Principal Technical Challenges	4
4. Development Activities	6
4.1 Evaluation of Target Application Concepts.....	6
4.2 Design Selection Process	6
4.3 Determining Heavy-Fuel Flameless Combustion Fundamentals	7
4.3.1 Validating Quantitative Properties of Catalytic Combustion	7
4.3.2 Light Fuel Testing/Calibration (Methanol and Ethanol).....	10
4.3.3 Heavy Fuel Testing/Calibration (Jet-A).....	11
4.3.4 Heavy Fuel Reforming.....	13
4.3.5 Dynamic Azeotrope Evaporator	16
4.3.6 Effects of Fuel Aging.....	22
4.3.7 Vibrating Shutter Nebulizer	26
5. Prototype Design and Construction	29
5.1 Preliminary System Design for the Flow-Through Water Heater	29
5.2 Subsystem Modeling, Design & Testing	31
5.2.1 Catalytic Combustor & Heat Exchanger Subsystem	32
5.2.2 Catalytic Combustion Chamber	37
5.2.3 Gas Flow and Heat Transfer Calculations	42
5.2.4 Flashback Analysis	44
5.2.5 Temperature Profile Inside Ceramic Combustor Plate	45
5.2.6 Catalytic Combustion Plate Surface Temperature	47
5.2.7 Catalytic Combustion Plate Physical Properties	47
5.2.8 Catalyst Deposition Profiles	49
5.2.9 Improved Catalytic Combustion Plate Properties	51
5.2.10 Catalytic Starter	55
6. Conclusions/Recommendations	71

List of Figures

Figure 1. Schematic of Experimental Set-Up	8
Figure 2. Catalytic Combustion Test Bed (left) & Evaporation Chamber (right)	9
Figure 3. Catalytic Combustion Data for Methanol & Ethanol	11
Figure 4. Catalytic Combustion Data for Jet-A Fuel	12
Figure 5. Schematic Showing Method to Reform Heavy Fuels into Simple Fuels	14
Figure 6. Catalytic Combustion Data for Jet-A Fuel	15
Figure 7. Schematic of Apparatus for Measuring Azeotrope Dynamics	18
Figure 8. Data Validating Dynamic Azeotrope Concept	19
Figure 9. Design Geometry Incorporating Dynamic Azeotrope Principle	20
Figure 10. Table-Top Dynamic Azeotrope & Catalytic Combustion Test Bed	21
Figure 11. Evaporative Body Showing Before & After Extended Use	21
Figure 12. Close-up of Test Surface After Running Contaminated Jet-A	24
Figure 13. Effect on Azeotrope from Aged & Contaminated Fuel	25
Figure 14. Effect on Azeotrope from Water Contaminated Fuel	25
Figure 15. Nebulizer Principle of Operation	26
Figure 16. Nebulizer Output Stream with Methanol or Jet-A	27
Figure 17. View of Nebulizer Head Assembled	28
Figure 18. System Design Concepts	30
Figure 19. Placement of TEG in Heat Flow Path	32
Figure 20. Inside Views of High Performance Heat Transfer Unit	33
Figure 21. Top and Bottom Views of Heat Transfer Unit	33
Figure 22. Example of Poor Heat Transfer Design	34
Figure 23. Significantly Improved Heat Transfer	35
Figure 24. Advanced Heat Transfer Prototype Performance	36
Figure 25. Pressure Drop versus Flow Rate	37
Figure 26. Combustor Temperature vs. Equivalence Ratio	38
Figure 27. Visualization of Fuel Droplet Size vs. Transport Effectiveness	39
Figure 28. Test Bed for Nebulizer-Based Catalytic Combustion	40
Figure 29. Alternative Air Moving Mechanisms Evaluated	41
Figure 30. Model Geometry for Gas & Heat Flow Estimates	42
Figure 31. Flow Tube Thermal Profile	44
Figure 32. Porous Ceramic Catalytic Combustion Plate Substrate	47
Figure 33. Diagram of Combustion Plate Experimental Apparatus	48
Figure 34. Pressure Drop versus Plate Parameters	49
Figure 35. Catalyst Gradient Strategies for Ceramic Substrate	50
Figure 36. View of Flow Uniformity Test Cell	51
Figure 37. Relationship Between Thermal & Electrical Conductivity	52
Figure 38. Metal Foam Combustor Plate Physical Structure	53
Figure 39. Thermal Conductivity vs. Primary Porosity of Combustor Plate	54
Figure 40. Thermal Conductivity vs. Temperature of Combustor Plate	55
Figure 41. Top View of Assembled Catalytic Starter Device	58
Figure 42. Close-up View of Ceramic Coated Filament w/Catalyst Applied	58
Figure 43. Catalytic Starter Cage Close-up	59
Figure 44. Microscopic View of Catalytic Starter “Light-Off” Promoter	60
Figure 45. Transient Temperature Calculations for 5 Volts	61
Figure 46. Transient Temperature Calculations for 10 Volts	61

Figure 47. Flow Chart Showing Areas of Potential Heat Transfer Improvements.....	63
Figure 48. Illustration of CAD Model Used in CFD Study.....	64
Figure 49. Reverberatory Screen Effect on Radiative Heat Transfer	65
Figure 50. Recuperative Heat Design Change.....	67
Figure 51. Illustrated Effect of Internal Convective Cell Formation on Fuel Delivery.....	68
Figure 52. Convective Cell Formation with Fully Developed Air Swirl Input	69

List of Tables

Table 1. Primary Milestones.....	4
Table 2. Heat Exchanger (HX) Test Results	35
Table 3. Fuel/Air Uniformity Experimental Results	51
Table 4. Fuel Temperature vs Fractional Boiling.....	57
Table 5. CFD Recommended Design Changes and Conclusions.....	71

Preface

Advanced Flameless Combustion Technology (AFCT) was originally conceived to address several consumer market segments in the outdoor industry. AFCT differs most notably from the earlier forms of catalytic combustion primarily by the “captive” (i.e., enclosed within an envelope) nature of the heat generating reaction. By enclosing the catalytic flameless reaction, Catalytic Devices International (CDI) has been able to demonstrate that substantial benefits can be accrued.

This report documents work performed for the AFCT Heavy Fuels Project by CDI during the period February 2006 to June 2008 under contract W911QY-05C-0064, awarded by the U.S. Army Natick Soldier Research, Development and Engineering Center (NSRDEC) under project element 622786. The project was directed toward the development of heavy fuels capability as a fundamentally new type of catalytic heat source based on the application of unique catalytic reaction and control principles established and patented by CDI.

These major competitive advantages are what distinguish AFCT and provide for new applications not previously possible with earlier catalytic combustion heat sources:

- System Weight
- Energy density
- Power Density
- Cost (both per unit and per watt-hour)
- Portability
- Packability
- Power Control

By exploiting the significant potential performance advantages in the categories above, it is felt that both civilian and military application of AFCT will benefit. Military application of AFCT are a logical extension of this technology, but they also challenge CDI to arrive at the optimum mix of features, performance and cost to satisfy the stringent demands of military application.

The specific tasks of this project, reported upon in the following pages, was to (a) advance the utility of AFCT such that it can operate from heavy fuels, such as JP-8, each adapted to the specific task required; and (b) increase the power output of AFCT to allow more types of physical and functional forms.

DEVELOPMENT OF AN ADVANCED, FLAMELESS-COMBUSTION HEAT SOURCE FOR USE WITH HEAVY FUELS

1. Summary

CDI's previous work on flameless combustion efforts were directed toward a variety of outdoor applications (including food heating) and medical applications using light fuels such as methanol, ethanol or butane. In combination with a variety of proprietary techniques and inventions, CDI has been successful in developing ultra-light, high powered, compact and safe variants of catalytic heat.

The general purpose of the work reported herein was to achieve catalytic heat generation using heavy fuels, applied toward Army specified needs, while maintaining attributes shown to be valuable and unique to lighter fuels.

This final report details the various results obtained and approaches taken to determine the feasibility of certain techniques to vaporize, transport, and catalytically oxidize heavy fuels. CDI performed this work, between February 2006 to June 2008, under contract to the U.S. Army Natick Soldier Research, Development and Engineering Center (NSRDEC).

The techniques that showed the most promise were developed further and utilized in a demo unit that provided portable flameless heat for a flow-through water heater intended as an accessory to a soldier's water hydration unit. System integration of some critical subsystem components developed in this project was performed, resulting in a prototype heating unit that demonstrated attributes of AFCT.

Specifically, the development effort was directed toward:

- Redesign of the (a) fuel vaporization subsystem, (b) the vapor transport subsystem, and (c) the reactor subsystem, such that each subsystem allows operation with heavy fuels (i.e., middle distillates) known as kerosenes such as JP-8, Jet A, and diesel.
- Scaling up (increasing) the heat power capability of AFCT to the one-kilowatt level to allow use in a variety of new applications.
- Demonstrate the potential benefits and advantages of AFCT by applying it to one or more of the specific Army needs.

This report is divided into two primary sections:

- The first section is devoted to research and testing that investigates basic properties and gathers relevant engineering data about subsystem components that will be needed for design, integration, and building of a prototype.
- The second section explains the design effort and the challenges faced, as well as the results obtained.

2. Introduction

While the catalytic combustion of kerosene fuels is known in the literature, the low temperature (e.g., 200 °C to 300 °C) catalytic combustion characteristic of AFCT, when applied to heavy fuels, is not and presents special challenges.

The effort was directed toward enhancement of CDI's current advanced flameless combustion technology so as to expand capabilities in two main technical areas:

- Fuel vaporization, vapor transport and catalytic flameless combustion of heavy fuels (i.e., middle distillates) known as the kerosene, such as, JP-8, Jet A and diesel
- Scaling up (increasing the heat power output to the 1-kW or 2-kW level to allow for a wider range of applications).

To reduce technical risk, CDI took more than one approach to the problem of vaporizing, transporting and catalytically oxidizing the fuel/air mixture. Heavy fuels require special consideration in each of these stages.

Approach #1: The vaporization process with heavy fuels can result in the build-up of residues or tar-like substances. Part of the project was devoted to extending the development of a fundamentally new class of vaporizers -- invented at CDI -- and referred to in this paper as Vapor Extraction Membrane (VEM) technique. The VEM technique in conjunction with other AFCT methods is uniquely qualified, for fundamental reasons, to tackle the difficult issues relating to residue build-up and vapor condensation with heavy fuels.

To achieve this, the development was aimed at: (a) designing a non-boiling evaporator with non-selective evaporation characteristics, (b) enhancing current VEM technology, and (c) empirical validation of non-selective evaporation.

Approach #2: The transport problem relates to the fact that heavy fuels have a much higher average boiling point than the normal fuels (alcohols and light fuels) used with CDI's current design. Several approaches to remedy this problem are available and have been investigated on a theoretical level at CDI. These include either individually or in combination the following techniques: counter flow heat transfer conduits, catalytically heated conduits, super-hydrophobic conduit walls. For practical reasons, and to mitigate schedule risk, a simple combination of heat conduit and short path transport was utilized for this project.

The ultimate purpose of vaporization and transport is to induce a catalytically supported fuel/air oxidation reaction (i.e., generate heat). CDI's current design needed modification to allow for the differences between the catalytic combustion properties of alcohols currently used and the heavy fuels, which contain unsaturated aliphatics, as well as saturated and unsaturated cyclic/multi-cyclic hydrocarbons.

Approach #3: The power-scaling task was accomplished by incorporating advances in low pressure high flow (LPHF) fan technology with a radical re-design of the reactor (i.e., catalytically coated combustion plate structure) to allow ultra-low back pressure and redistribution of the heat energy in conjunction with solutions to vapor transport of saturated fuel/air mixtures as presented below.

In the later part of the project, CDI teamed up with the Creare Inc. in an effort that centered around combining Creare's fuel nebulizer system with CDI's catalytic combustion sub-systems.

To achieve a smooth alignment of the two technologies, CDI undertook the task of providing detailed mathematical modeling of the prototype. This allowed for rapid adjustments to the prototype when performance issues arose. Ultimately, it also provided a future direction for an eventual re-design of the prototype for possible market entry.

3. Milestones and Timeline

3.1 Overview of Significant Project Milestones

Table 1 provides an overview of the project.

Table 1. Primary Milestones

	Project Milestones		
	2006	2007	2008
Heavy Fuels Catalyst Testing Facility Completed			
Analysis of Target Applications Completed			
Flow-Through Water Heater Application Design Concept Completed			
Catalytic Reforming Alternative Approach			
Dynamic Azeotrope Alternative Approach			
Effects of Fuel Aging on Catalytic Performance Analyzed			
Ultrasonic Nebulizer Approach Established as Primary Technique for Project			
All Subsystems Modeled and Designed			
Subsystems Fabricated and Tested			
Subsystem Integration Completed			
System Performance Modeled and Improvements Made			

3.2 Principal Technical Challenges

There were two primary areas of technical challenge that upon reflection can be determined to be the driving elements for project resources. They are:

- maximizing the cross-over of established technical solutions from the proven CDI light fuels technology towards the catalytic combustion of heavy fuels, and
- adapting the heavy fuels solution to a specific Army field application.

While the catalytic combustion of kerosene fuels is known in the literature, the low temperature catalytic combustion (e.g., 200 °C to 300 °C) characteristic of AFCT is not and presents special challenges.

Part of the development effort reported herein was directed toward a significant enhancement of the current advanced flameless combustion technology at CDI. The effort was directed toward enhancement of capabilities in two main technical areas:

- fuel vaporization, vapor transport and catalytic flameless combustion of heavy fuels (i.e., middle distillates) known as the kerosene, such as, JP-8, Jet A, and diesel; and
- scaling up (increasing) the heat power to the kilowatt level with a wider range of applications.

To reduce the technical risk, CDI took several different approaches to the problem of vaporizing, transporting and catalytically oxidizing the fuel/air mixture.

The extension of the “Vapor Extraction Membrane” (VEM) to operate with JP-8 was a primary effort in the early part of the project. VEM is unique to CDI and was originally developed for outdoor products to allow relatively high chemical power levels in a very compact unit.

A JP-8 version of VEM was shown to be viable through the use of table-top “proof of principle” experiments. However, it was not brought close enough to a product level in time for implementation in a field version during the project.

Instead, for the purposes of reducing schedule risk, a method known as vibrating-mesh nebulizer was adapted since it was already in a relatively advanced state at the time. However, the nebulizer introduced a host of new challenges having to do with completing the vaporization, mixing of fuel with air and metering the fuel in a reliable fashion. It also required that a new type of catalytic combustor plate be developed, with thermal and catalytic properties that are amenable to the nebulizer characteristics.

Finally, a more complete understanding of the complex behavior underlying the demo unit was needed because of several unexpected outcomes during testing of the demo unit. The subsystems that make up the demo unit were analyzed both in singular form and as an assembly in a completed system. The results provided corrective actions that were applied to the final unit.

4. Development Activities

Sections 4.1 through 4.3.7 represent the gathering of fundamental engineering data and research that was used in section 5 for the building of the demonstration unit sub-systems.

4.1 Evaluation of Target Application Concepts

Early in the project an attempt was made to establish a realistic goal for directing the research. This was done by calculating high level engineering and physics parameters associated with each particular goal.

A number of potential applications were evaluated to determine the best one for showcasing the technical results of the project. Detailed calculations were performed and design criteria established regarding performance for the following potential catalytic applications:

- Snow melter to melt 1.5 kg of snow, and heat it to 70 °C
- Immersion water heater to heat 500 gm of water to 70 °C
- "Instant" (flow-through) water heater to heat water to 70 °C
- Hotplate to heat 500 gm of water to 70 °C

Ultimately, the Instant Water Heater (IWH) was chosen as being best suited for demonstration in the time and budget allotted.

4.2 Design Selection Process

An analysis of total energy, power required for reasonable heating times, amount of fuel and air (and their flow rates) required for each application, along with the amount, rate, and composition, and physical characteristics of exhaust products, all lead to a recommendation for a particular target application.

Vapor pressure calculations and the results of experiments were used to determine the thermal requirements of the evaporator and catalytic reactor components. These results were then be used to examine materials compatibility issues.

During the consideration of the various target applications, the analysis was incorporated using the following criteria:

- The heated components within the evaporator and combustor will be fabricated from materials capable of operating at temperatures in excess of 400 °C.
- The area of all heated components will be minimized to minimize startup heat requirements.
- The thickness of all heated components will be minimized to minimize startup heat requirements.
- The specific heat capacity of all components will be minimized to minimize startup heat requirements.

- The heat transfer path between the catalyst and the heated surface must consist of an insulating material in order to maintain the catalyst at high temperature.
- A heat recuperator should be employed to heat the incoming air and cool the exhaust, thereby maximizing efficiency.
- The external surface area of the device will be minimized in order to minimize heat loss.
- Per-use fueling should be considered due to the very low volume of fuel required for each use.
- Utilization of a collapsible air bladder should be considered due to the relatively low volume of air required for each use.

The above results were then used to perform a preliminary design analysis for the devices listed, and to make recommendations for the direction of development efforts.

The conclusion was that the best target application to showcase the research results would be a catalytic flow-through water heater.

4.3 Determining Heavy-Fuel Flameless Combustion Fundamentals

The catalytic oxidation of the simple fuels like methanol and other aliphatic hydrocarbons are relatively well characterized in the literature. JP-8, which contain a wide range of hydrocarbon species are not readily predictable from first principles over the wide range of temperatures desired, and thus needed to be examined to obtain a good working knowledge of the process. This basic data would later allow us to design the elements that go into a JP-8 catalytic reactor.

4.3.1 Validating Quantitative Properties of Catalytic Combustion

The combustion of heavy fuels in AFCT devices poses additional challenges to the AFCT technology. Such fuels are both chemically complex, being composed of complex molecules, and chemically heterogeneous, comprising a mixture of hundreds of different complex molecular species. These complexities will result in the production of a tremendous diversity of intermediate compounds as well as the possibility of side (non-oxidative) reactions. In addition, significantly higher catalyst temperatures are likely to be required for complete oxidation.

The oxidation reaction between fuel and oxygen requires that the molecules have a minimum kinetic energy in order to approach closely enough to react and then break the existing bonds between the atoms so that new bonds can be formed. This energy is called the "activation energy." The kinetic energy of the molecules can only be increased by increasing the temperature of the fuel-air mixture. This is why a spark is needed to light a flame.

The advantage of a catalyst is that the molecules stick to the surface of the catalyst particles and the attractive forces between the atoms of the catalyst and the atoms in a fuel molecule cause the bonds to stretch so that less energy is required to break the bonds -- i.e., the temperature of the fuel-air mixture (and the catalyst) required for combustion to occur can be much less than the temperature of a flame.

It is still true, however, that a higher temperature will result in a higher reaction rate -- the catalyst simply lowers the temperature at which the reaction begins. In addition, a molecule like

methanol must undergo multiple reactions in order for complete oxidation to occur -- the reaction is not just one step as might be assumed from the appearance of the overall reaction formula:



For simple fuel molecules, such as methanol, a relatively low temperature can produce complete oxidation since the bonds in a methanol molecule are stretched very effectively by the platinum catalyst and also because each methanol molecule must participate in only a few reactions to become completely oxidized. With more complex molecules, such as dodecane ($\text{C}_{12}\text{H}_{26}$ -- a component of jet-fuel) many more reactions must occur, and some of those reactions also have higher activation energies. So we expect that higher temperatures will be required to combust heavy fuels as compared to methanol.

To understand and quantify these challenges, it was necessary to construct an experimental apparatus that allowed for the quantitative measurement of the degree of catalytic oxidation for a given fuel as a function of temperature. **Figure 1** shows the schematic of the apparatus used to extract the experimental data.

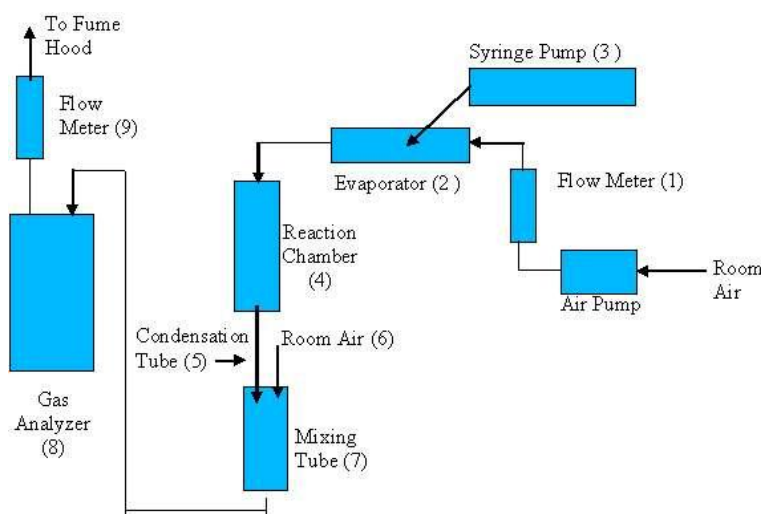


Figure 1. Schematic of Experimental Set-Up

The catalytic reactor module was designed to provide:

- (a) A sealed reaction chamber containing a flow channel and entry/exit fittings
- (b) A catalyst support on one wall of the chamber that is approximately isothermal. This is required so all portions of the catalyst zone are at nearly the same temperature, thus allowing a measurement of the degree of combustion as a function of temperature. Measurements of oxidation rates were taken at 10 °C intervals. The uncertainty in the catalyst temperature was kept to less than 10 °C to insure that the data are meaningful.

(c) A catalyst support that is of sufficient size so as not to be diffusion-limited. That is, substantially all fuel molecules must be able to move by diffusion across the channel to the catalyst surface before exiting the chamber.

Diffusion limits are important because the fuel-air mixture enters one end of the chamber, flows through the chamber, and exits the far end. Only molecules that actually strike the inner wall of the chamber coated with catalyst can be oxidized. Since the bulk flow is parallel to the wall, by itself, it cannot cause molecules to strike the catalyst. That job is done by diffusion, the random motion of individual molecules.

The average distance a molecule diffuses during a given time interval can be calculated. It is called the diffusion length. If the diffusion length is large compared to the largest distance that a molecule needs to travel in order to strike the catalyst-coated wall, then diffusion will not be a limiting factor. In that case, temperature will be the only determinant of the amount of the fuel that is combusted as the mixture flows through the chamber.

Requirement (b) above dictates that a high thermally conductive material be used for the chamber and that the cross-sectional area of the chamber be sufficient so that, taking into account the heat power generated by combustion and also the length of the flow channel, the temperature difference between the ends of the channel is less than the desired temperature uncertainty.

Requirement (c) dictates that the height of the channel be small enough that -- taking into account the gas flow velocity, the chamber length, and molecular diffusion coefficient -- the resulting (lateral) molecular diffusion length will be much larger than the channel height.

A physical implementation of the schematic is shown in **Figure 2**, where the combustion chamber on the left is disassembled to show the catalyst strip undergoing testing and the evaporator on the right side of the image illustrates how the fuel is fed into the evaporation chamber (via a syringe pump) before being transported to the catalytic combustion unit.

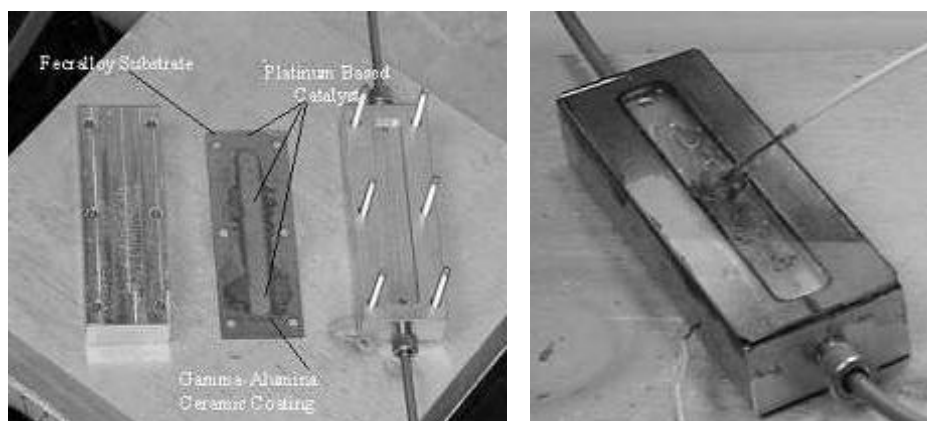


Figure 2. Catalytic Combustion Test Bed (left) & Evaporation Chamber (right)

The rate of feed of the syringe pump is controlled by a computer program to allow a precise control and measurement of the fuel/air mixture entering the flameless combustion unit. Both the evaporation unit and combustion unit are maintained in an isothermal condition by way of thermostatically controlled heat sinks.

In preparation for testing of the target fuel, JP-8, simple aliphatic alkane molecules (i.e., methanol & ethanol) were first used to calibrate and test the concept and apparatus to determine the degree of combustion as a function of temperature.

4.3.2 Light Fuel Testing/Calibration (Methanol and Ethanol)

Because methanol and ethanol are volatile at room temperature, a bubbler was temporarily substituted for the fuel vaporizer unit shown in **Figure 2**. Room air was bubbled through the liquid alcohol fuel maintained at an approximately constant temperature, thereby producing a known fuel/air mixture. The temperature of the reaction chamber was varied by use of the thermostatically controlled heat sink (hot plate). During some data runs, the chamber was placed on a block of thermal insulator material, allowing the temperature to vary slowly (about 2 °C per minute) downward by ambient air cooling.

The following experimental variables were measured:

t	Time of measurement
T _{cat}	Temperature of catalytic combination chamber [Celsius]
T _{bub}	Temperature of liquid in bubbler [Celsius]
O ₂	Oxygen concentration in exhaust gas [volume percent]
HC	Hydrocarbon concentration in exhaust gas [ppm]
F _a	Flow rate of dilution air (used to prevent condensation in the gas analyzer) [ml/min]
F _f	Flow rate of air into bubbler containing methanol or ethanol [ml/min]

Due to the temperature dependence of the catalytic oxidation process, we expect the following behavior:

At low temperature there should be no reaction; therefore, the oxygen concentration should remain at the atmospheric value of 20.9% and the hydrocarbon value should be at the input concentration (i.e., the plateau in the graph of concentrations vs. temperature at low temperatures). At sufficiently high temperatures there should be another plateau, this time with the oxygen concentration at a lower value than atmospheric and the hydrocarbon value at zero. Between the low and high temperature plateaus we should see a transition in which partial oxidation occurs (along with possible side reactions). If no high-temperature plateau occurs then the oxidation is not complete.

During the run, the bubbler temperature varied between 24.9 and 25.1 °C. The bubbler input air flow was constant at 31 ml/min and the dilution air flow was constant at 800 ml/min. The measurements were commenced at T_{cat} of 80 °C and terminated at 30 °C.

The measured values of O₂ and HC concentrations are given below in **Figure 3**.

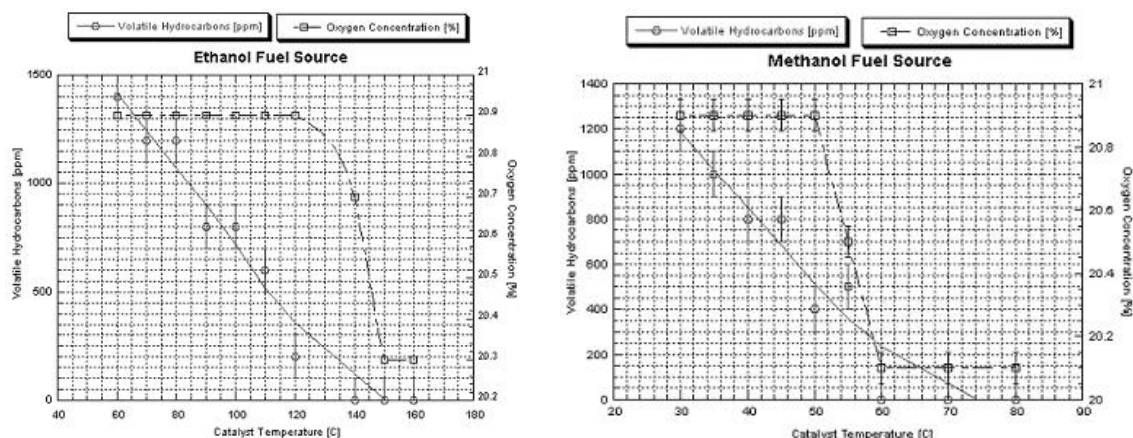


Figure 3. Catalytic Combustion Data for Methanol & Ethanol

4.3.3 Heavy Fuel Testing/Calibration (Jet-A)

The experimental apparatus having been tested and calibrated, as shown above, was then employed to measure the degree of combustion as a function of temperature for Jet-A type fuel.

Room air was pumped through the evaporator at 48 ml/minute and dodecane was injected at 0.25 ml/hour, yielding a mixture that is 85% of stoichiometric (slightly lean). The temperatures of the reaction chamber and the evaporator were varied by use of the hot plates.

The following experimental variables were measured:

t	Time of measurement
T _{cat}	Temperature of catalytic combustion chamber [Celsius]
T _{evap}	Temperature of evaporation chamber [Celsius]
O ₂	Oxygen concentration in exhaust gas [volume percent]
HC	Hydrocarbon concentration in exhaust gas [ppm]
F _a	Flow rate of dilution air (used to prevent condensation in the gas analyzer) [ml/min]
F _f	Flow rate of fuel [ml/min]

Due to the temperature dependence of the catalytic oxidation process, we expect the following behavior:

At low temperature there should be no reaction and so the oxygen concentration should remain at the atmospheric value of 20.9% and the hydrocarbon value should be at the input concentration. This will show up as a plateau in the graph of concentrations vs. temperature at low temperatures.

At sufficiently high temperatures there should be another plateau, this time with the oxygen concentration at a lower value than atmospheric and the hydrocarbon value at zero. Between the

low and high temperature plateaus we should see a transition in which partial oxidation, along with possible side reactions, occurs. If no high-temperature plateau occurs then the oxidation is not complete.

During the data run, the evaporator temperature was maintained at 189 °C, and the catalyst chamber temperature was varied from 275 to 205 °C in 5° increments. The dilution air flow was constant at 900 ml/min.

The resulting measured values of O₂ concentration as a function of catalyst temperature are given in **Figure 4**. The results are simple to interpret: partial oxidation began between 240–250 °C and oxidation was complete between 260–270 °C, as revealed by the low and high temperature O₂ concentration plateaus.

Based on data like these and many other similar experiments, it was determined that a low temperature catalytic oxidation can be carried out to completion for Jet-A type fuels without coking or contaminate poisoning of the CDI type catalyst.

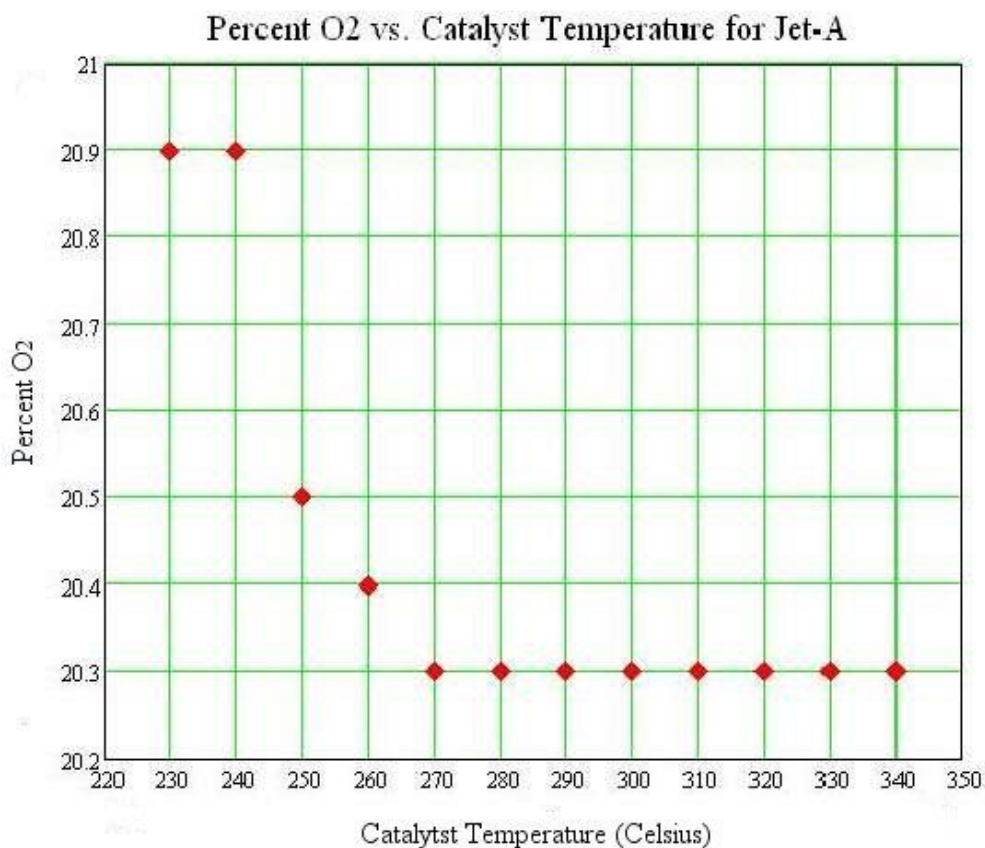


Figure 4. Catalytic Combustion Data for Jet-A Fuel

4.3.4 Heavy Fuel Reforming

A significant challenge for heavy-fuel AFCT devices is the requirement that the entire catalytic combustor be preheated to a temperature of over 300 °C prior to the initiation of fuel and air flow.

Another difficulty with the evaporation and combustion of Jet-fuel is that the evaporation must be accomplished in close proximity to the combustion, because the fuel-air mixture from the evaporator will have a high dew point of about 200 °C. Transport of the fuel-air mixture between a separate evaporator and combustor would require that the transport path be maintained at a high temperature, which would, in turn, require bulky (and inflexible) thermal insulation as well as a method of raising and maintaining the high temperature.

It is possible to maintain the heat along the pathway by performing partial oxidation reactions throughout the conduit. At this stage of development, in order to maintain schedule it was decided this approach could be revisited at a later time -- after first designing and testing the basic system.

The above limitations make the evaporation and catalytic combustion of jet-fuel significantly more difficult than, for example, methanol. A technical approach that may circumvent these limitations would be to include a device that could convert the jet-fuel into a different liquid fuel having a much lower boiling point. This would eliminate the problem of condensation and which would catalytically oxidize at a relatively low temperature.

In conforming with the methodology outlined at the beginning of the report, multiple approaches to solving a problem would be explored when feasible.

One such alternate approach is a fuel processing technique known as "fuel reforming." There exists a considerable technological data base that would allow the development of reformers using jet-fuel. The reformer would output a product known as "synthesis gas" or "syngas," -- an equimolar mixture of hydrogen and carbon monoxide.

This type of fuel processor is also known as a partial oxidation reformer. The integration of such a reformer with the evaporator would result in a fuel that would remain a gas down to about -200 °C, thereby enabling easy transport over an arbitrary distance to the combustor.

The question of the temperature required to allow complete catalytic combustion of the syngas was explored. To answer this question, we conducted experiments using proprietary CDI catalyst technology.

To determine the temperature required to completely combust syngas, it is necessary to construct an apparatus that will allow for a quantitative measurement of the extent of catalytic oxidation for a given fuel as a function of temperature.

In addition to the combustion chamber described in the preceding section, the following equipment was used to construct the experimental apparatus:

- (1) compressed-hydrogen gas tank and pressure regulator
- (1) carbon-monoxide (CO) gas tank and pressure regulator
- (1) room-air compressor and pressure regulator
- (3) Dwyer flow meters with adjustable needle valves
- (1) Test Products International model 712 flue gas analyzer
- (1) Corning model PC-351 hotplate
- (1) Keithley model 873C thermocouple meter with a type-K thermocouple

The flow of gases between these components is shown schematically as in **Figure 5** below.

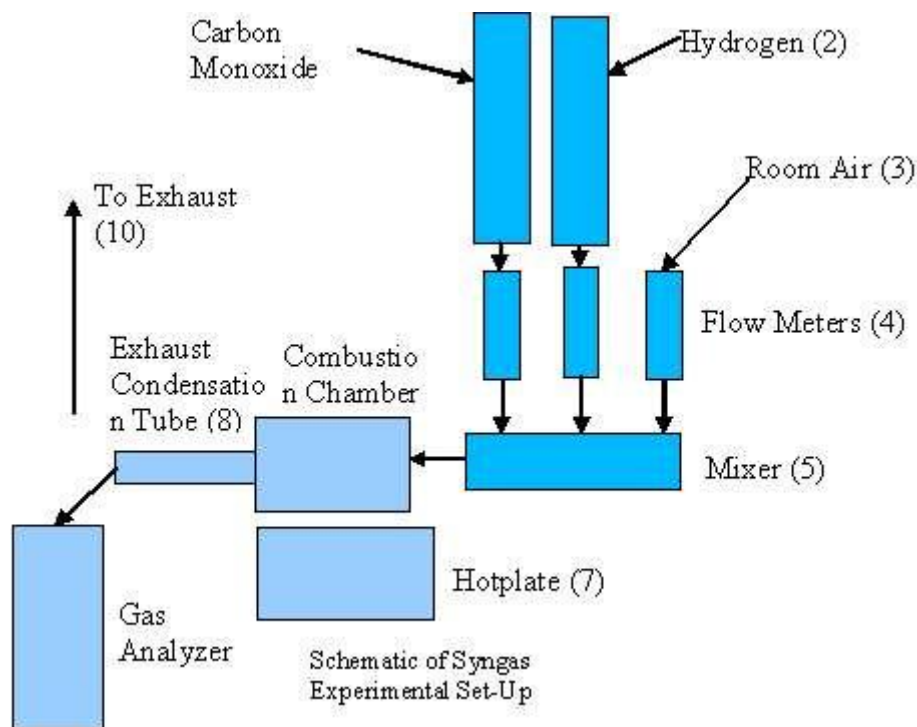


Figure 5. Schematic Showing Method to Reform Heavy Fuels into Simple Fuels

The experimental apparatus described above was employed to measure the degree of combustion as a function of temperature for synthesis gas. Three data sets were captured:

- CO + air,
- H₂ + air, and
- CO + H₂ + air.

The following subsections describe the experimental results for these three mixtures.

Carbon-Monoxide + Air:

The first experiment used a lean (80 ml/min air and 10 ml/min CO -- equivalence ratio = 0.3) mixture of air and CO. It is well known that CO has a high affinity for platinum and so we expect that this mixture will require a high temperature to begin combustion.

We concluded that the CO/air mixture requires temperatures in the range of 300 °C for substantially complete combustion.

H₂ + Air

The second data set was acquired using an approximately stoichiometric mixture of air and hydrogen (100 ml/min air and 40 ml/min hydrogen -- equivalence ratio = 0.96).

A small platinum catalyst sensor was inserted into the end of the exhaust condensation tube to serve as a rough combustible gas sensor. The hotplate was turned on and set to a ramp rate of about 3 °C per minute. The sensor indicated the presence of H₂ exhaust until a temperature of 75 °C was reached.

CO + H₂ + Air (Syngas)

For the combustion of synthesis gas we would expect that the temperature required for substantially complete combustion would be between the (high) temperature found for CO + air and the (low) temperature found for H₂ + air. To determine this temperature, we used a slightly lean mixture (250 ml/min air, 42 ml/min CO, and 42 ml/min H₂ -- equivalence ratio = 0.8).

The experiment was begun at 140 °C with the hotplate set to a ramp rate of about 3 °C/min. The probe of the gas analyzer was inserted at 160 °C and left in place. The CO sensor reading was not used due to the high (off-scale) concentration of CO. The O₂ sensor readings as a function of temperature are depicted in the graph shown in **Figure 6**.

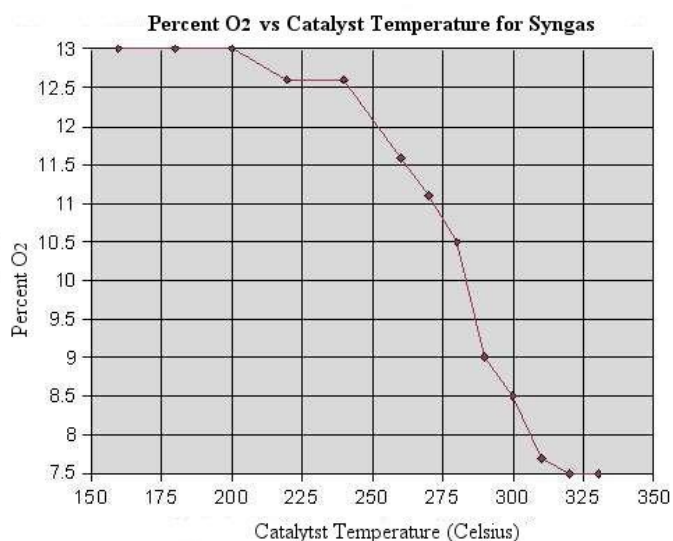


Figure 6. Catalytic Combustion Data for Jet-A Fuel

This demonstrated that syngas created from jet-fuel by means of a partial oxidation reformer would eliminate condensation in transfer lines between the evaporator/reformer and catalytic reactor.

However, the catalyst temperatures required to combust syngas are in the same range as for catalytic combustion of jet-fuel vapor using the current catalyst. Therefore, the use of flexible materials -- typically requiring temperatures less than 200 °C -- which are desirable for implementing AFCT, are problematic when using syngas.

CDI is working on new designs for extending AFCT to these higher temperatures while retaining all of the flexibility, lightweight and surface-conforming features.

Because of progress in these two areas, the advantage of nearly unlimited transport of the gaseous fuel/air mixture, without condensation issues, may be significant enough to warrant a revisit of the reforming approach in the future.

4.3.5 Dynamic Azeotrope Evaporator

The methodology explored next is directed toward extending the currently successful method utilized at CDI with simple fuels, to be applicable to heavy fuels.

Evaporation of jet-fuel is considerably more difficult than evaporation of a pure liquid, such as methanol, due to several factors:

- Jet-fuel is a complex mixture of literally hundreds of chemical compounds with different boiling points, resulting in a boiling temperature *range* instead of a sharp boiling point.
- Evaporation of such a mixture generally results in a change in composition of the fuel and vapor over time (distillation), since the low-boiling components tend to evaporate early in the process.
- Jet-fuel contains chemical species, such as olefins, that are reactive and can cause degradation of the fuel, especially when the fuel is in contact with air, heat, and/or light. The degradation consists of the production of new fuel components that have very low volatility or may be non-volatile.
- Jet-fuel can contain particulate matter.
- The composition can vary from batch to batch, since the feedstock from which it is produced is of natural origin.

The problem posed by distillation is that the temperature and composition of both the liquid and vapor will generally change over time. This makes the constant power output operation of the combined evaporation/combustion system difficult or impossible. For example, if air is bubbled through a heated volume of jet-fuel, the resulting fuel-air mixture will contain an excess of the low-boiling fuel components. As these light components are distilled off, the temperature of the liquid must be increased in order to maintain the air-fuel mixture (known as the equivalence ratio) within the design range of the combustor.

This problem does not exist for a special type of mixture known as an *azeotrope*. An azeotropic mixture has the property that the composition of the liquid and the vapor remain constant during evaporation. The most well-known of these mixtures is the combination of 95% ethanol and

5% water. Unfortunately, jet-fuel is not an azeotropic mixture and actually has a relatively wide boiling range, beginning at 180 °C and ending at 260 °C.

It is possible to design an evaporator that produces a dynamic azeotrope, resulting in a system in which the composition of the vapor is identical to that of the fuel. This would then assure a constant evaporation temperature and vapor composition.

A dynamic azeotrope will occur in an evaporation system that possesses the following attributes:

- Evaporation takes place at a stable liquid-vapor boundary.
- The flow of liquid fuel from the fuel reservoir to the boundary is laminar (i.e., no turbulence or other mixing effects occur) and entirely directed toward the boundary.

In such a system, when evaporation begins the composition of the liquid at the liquid-vapor boundary will change as low-boiling components evaporate, leaving higher-boiling components in the liquid. The requirement of laminar flow toward the boundary prevents the higher-boiling components from being carried back to the supply, except by the process of molecular diffusion. The balance of liquid flow toward the boundary and diffusion of heavy fuel components away from the boundary will result in a stable concentration gradient that can be confined to a region near the liquid-vapor boundary. A stable composition at the boundary, in turn, results in a vapor composition which is identical to the composition of the fuel in the reservoir.

In other words, the liquid at the boundary becomes enriched in heavy fuel components and increases in temperature until the heavy components reach a particular composition and temperature, causing an evaporation rate balancing the rate that heavy components are delivered by the liquid to the boundary. When such a stable composition and temperature steady state is achieved, a dynamic azeotrope has been created.

The dynamic azeotrope is achieved by the balance of liquid flow toward the liquid-vapor boundary and the diffusion of high-boiling components away from the boundary (i.e., toward the fuel reservoir). If the heat required to evaporate the liquid is applied only at the liquid-vapor boundary, another balance will automatically be achieved: a balance between heat conducted through the liquid from the boundary toward the reservoir and the cold liquid flowing toward the boundary. This will produce a temperature gradient such that the heat producing the evaporation will not propagate to the fuel reservoir.

In addition to the two design requirements identified above, it is also necessary that the system reach a dynamic azeotrope steady state in a short time relative to the operation time of the evaporator. This is important, because during this start-up interval the temperature and composition of the fuel will be varying. This can be achieved by requiring that the fuel volume contained in the evaporator porous media be a small fraction of the total fuel volume in the reservoir.

A pictorial diagram, illustrating the set-up of the evaporation test platform used for this research, is shown in **Figure 7**.

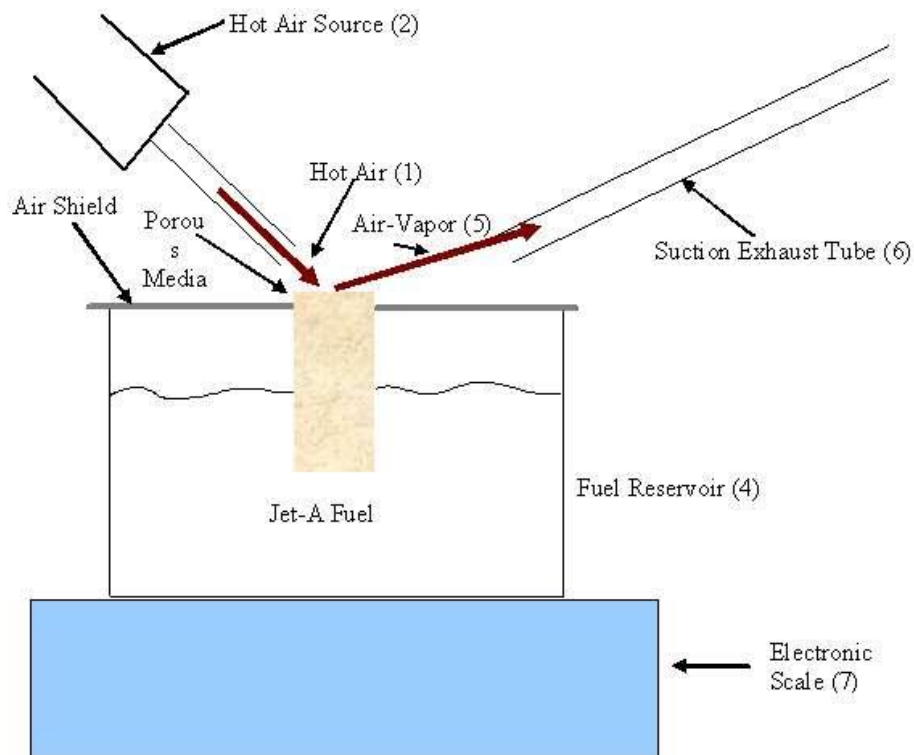


Figure 7. Schematic of Apparatus for Measuring Azeotrope Dynamics

The evaporator design requirements described above can be satisfied by the use of a chemically inert porous material which can withstand the high temperatures ($>200\text{ }^{\circ}\text{C}$) necessary for jet-fuel evaporation. Such a material was used to fabricate a cylindrical porous wick that resulted in a stable liquid-vapor boundary. The intrinsic capillarity of the material draws in the fuel and completely saturates it. Fuel can be brought into contact with one end of the cylinder, and heat applied to the opposite end to produce evaporation.

In a practical implementation of this technique, the heat of vaporization would be applied from a localized partial catalysis of the fuel vapor. Also, the surface of the porous material would be treated to be super hydrophobic to allow any orientation without liquid fuel dripping from the surface. Alternatively, a pressure difference between the reservoir and the wick can be maintained artificially to allow un-restricted orientation of the device.

For test purposes, the simplest method of applying both heat and air flow to the boundary is by preheating the air and flowing the air over the evaporation surface of the wick. To produce a well-controlled air temperature and manually select the air-stream speed, a regulated hot-air station was purchased and modified for this experiment. The device provides hot air at controlled temperatures that can exceed $400\text{ }^{\circ}\text{C}$ and at controlled flow rates of more than 20 liters/min.

The evaporator wick is fabricated from Zircar ZAL-45AA, a porous alumina, which is usually used for high-temperature furnace insulation. The cylindrical wick was sealed to prevent evaporation from the sides by the application of a layer of a thin layer of glass glazing. The glazing has a coefficient of thermal expansion that is matched to the porous material. The top and bottom surfaces of the wick were left unsealed. This wick design can withstand temperatures of over 700 °C if necessary.

The amount of heat delivered to the boundary is determined by the velocity and temperature of the hot air, which is held constant during the experiment. The development of a dynamic azeotrope will be signaled by the following process characteristics:

- A transient period in which the temperature of the boundary increases as the high-boiling fuel components become concentrated at the boundary.
- A steady state in which the temperature of the boundary is constant.

If the fuel is degraded by non-volatile components, then the steady state will be replaced by a pseudo-steady state in which the liquid-vapor boundary temperature increases at a particular rate. This slow temperature increase is caused by the gradual accumulation of an assortment of fuel components (i.e., different molecular weights) at the boundary. If these components have moderately low-volatility, then the boundary temperature will eventually level off to a new equilibrium. If the accumulation consists largely of non-volatiles (e.g., sludge), a continuous temperature increase will result.

The resulting temperature of the hot air stream (top trace) and the evaporation boundary (bottom trace) are recorded in **Figure 8**. This data validates the concept.

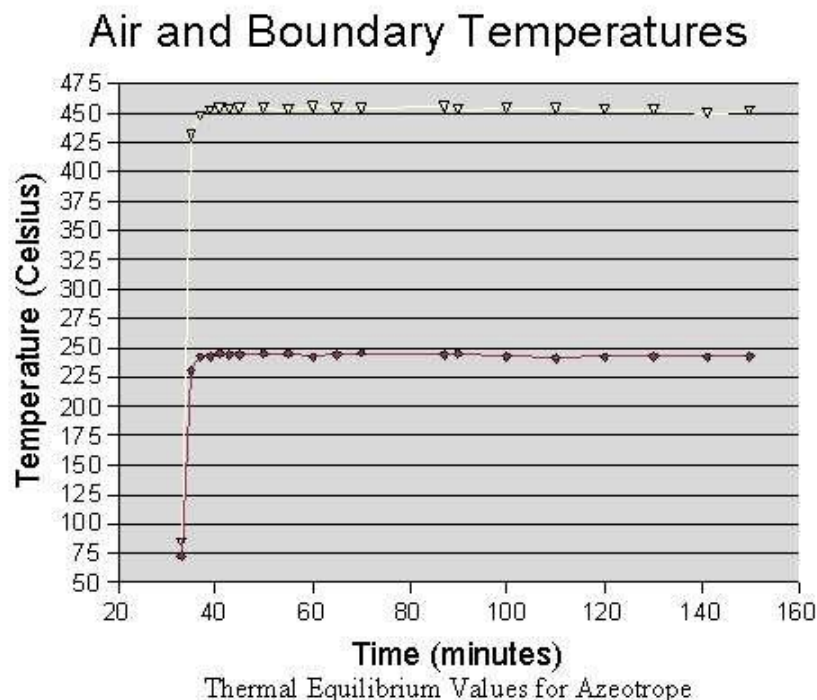


Figure 8. Data Validating Dynamic Azeotrope Concept

The top portion of the graph in Figure 8 showed that thermal energy was being delivered at a steady rate. Any variation in this rate would be expected to show up as a variation in the bottom portion of the graph. Subtracting the difference between the two data sets and differentiating provides a measure of azeotrope drift rates. The resulting drift rate, within experimental error, was found to be zero.

These results indicate that a dynamic azeotrope is successfully achieved, and that no significant increase occurred in the azeotrope equilibrium temperature after the first hours of evaporation.

Consequently, it appears that this evaporation methodology can be employed to provide effective jet-fuel evaporation for periods exceeding of tens of hours.

To determine if a stable dynamic azeotrope can be established in a practical and efficient evaporator design, it was desirable to design an evaporator for which the evaporation rate is approximately constant over the evaporating surface.

For a practical evaporator, it is important that the air-fuel flow be enclosed in a channel instead of using the unbounded approach taken in the design of the experimental evaporation apparatus. Since the evaporation rate is a function of temperature, as well as fuel-vapor concentration and boundary-layer thickness, such a design will require a flow channel whose thickness decreases so as to increase the air-fuel velocity along the flow direction.

A basic conceptual cylindrical design incorporating these features is illustrated in **Figure 9**:

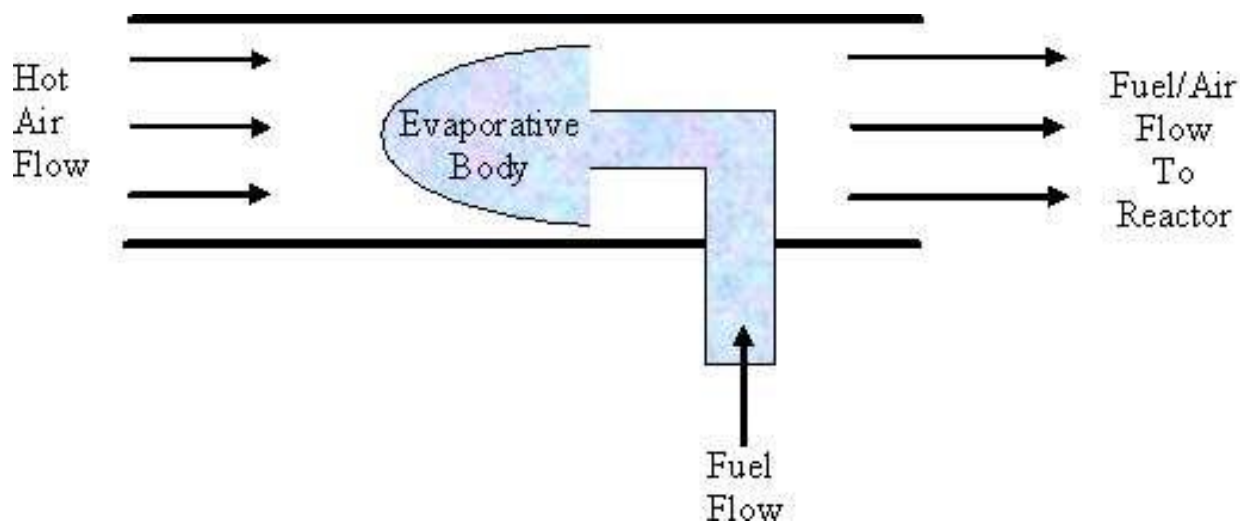


Figure 9. Design Geometry Incorporating Dynamic Azeotrope Principle

Several evaporative bodies of the half-ellipsoid shape shown in Figure 9 were fabricated using a variety of porous aluminas from Zircar. One with a diameter of 17 mm and length of 22 mm was bonded to a Pyrex tube to provide a connection to the fuel reservoir, installed in the apparatus shown in **Figure 10**, and run for 10 to 20 hours.

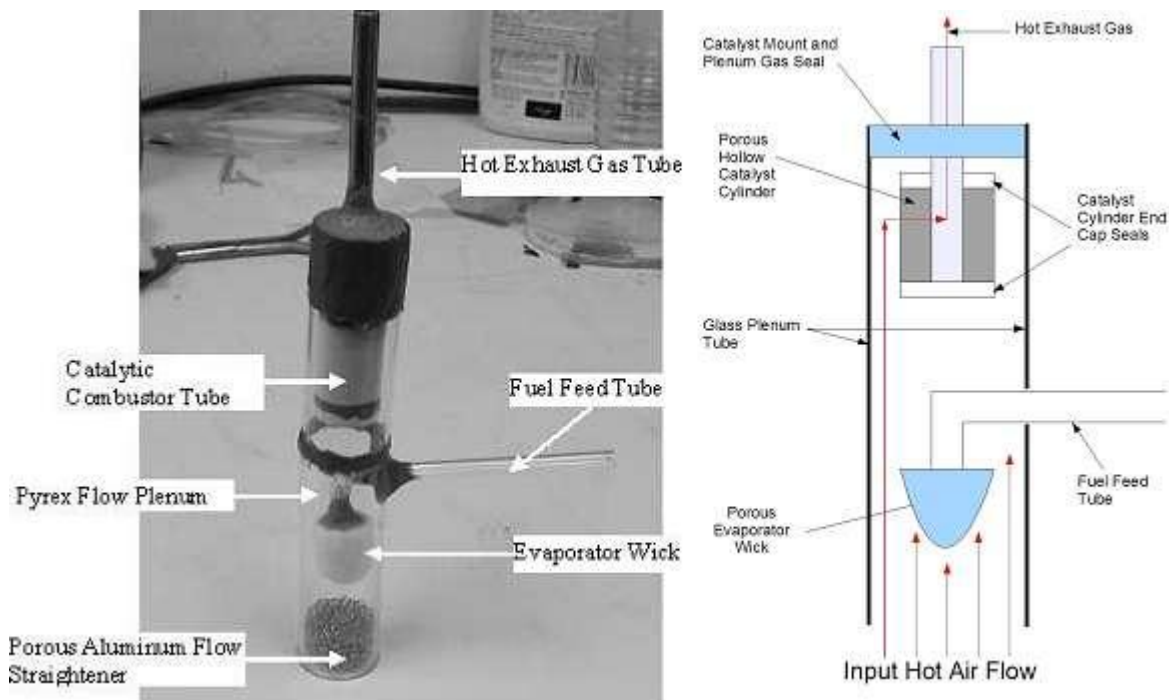


Figure 10. Table-Top Dynamic Azeotrope & Catalytic Combustion Test Bed

The fuel reservoir was placed on a sensitive scale to monitor the evaporation rate. The evaporative body was enclosed by a Pyrex tube with an inner diameter of 23 mm. The tube was press-fit onto the hot-air source by the use of Teflon tape as a gasket. A cylindrical piece of reticulated aluminum open-cell foam was inserted into the Pyrex tube above the hot-air source to serve as a flow-straightener, since the output of the hot-air source was found to be highly non-uniform.

Figure 11 shows the evaporative body before and after the 20 hours of operation, and illustrates the discoloration that results when either accelerated aged fuel or purposely contaminated fuel is used. The cross-sectional view on the right shows an axially symmetric discoloration. It is

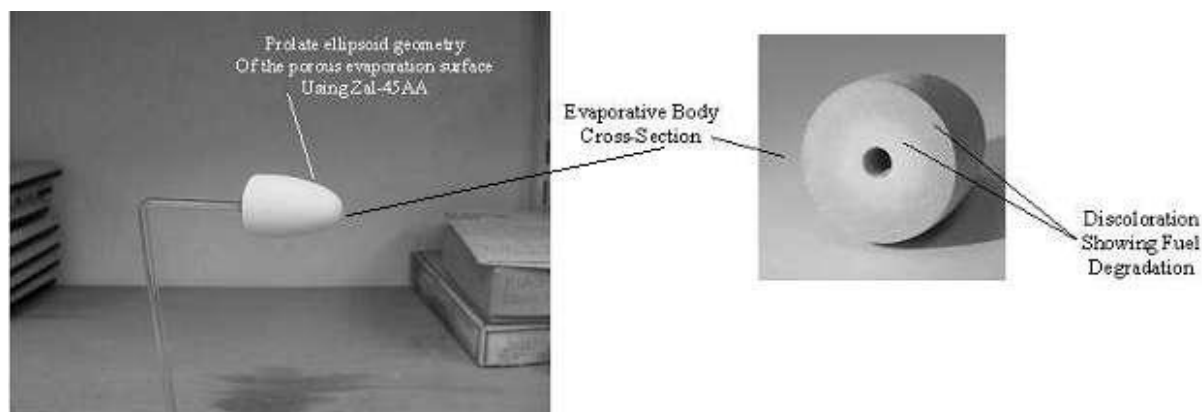


Figure 11. Evaporative Body Showing Before & After Extended Use

believed that this occurs as a result of a very mild catalytic reaction between the alumina wick material and the fuel. Some of the fuel's molecular components are believed to have been slowly converted to higher molecular weight compounds that are non-volatile and become attached to the alumina fibers. The lighter areas of the wick are marked by a subtle small-scale pattern that we theorized may be due to phase separation and/or the Marangoni Effect. The large-scale pattern may be due to the highly non-uniform hot-air velocity and temperature distribution over the wick surface, which would cause its own Marangoni flow (surface tension decreases with increasing temperature). It is likely the non-uniform hot-air flow is responsible for at least a portion of the deposition.

To test this hypothesis, a similar evaporative body was constructed using Ferro 3249 silica powder, formed and sintered into a suitable shape

The silica evaporative body was then run through the same fuel evaporative testing as the alumina body. The results showed no detectable discoloration of the evaporative body, lending support to the hypothesis that surface chemistry in the alumina was altering the fuel composition.

The silica has other properties that reduce the possibility of chemical interaction. In particular it has a much lower thermal conductivity -- this lowers the temperature experienced by the fuel during transport to the evaporating surface -- and it has a microstructure absent the filaments or whiskers found in alumina. The absence of filaments is important, because filament structures provide a higher surface area for reactions to occur upon.

4.3.6 Effects of Fuel Aging

We now describe the results of the effects of fuel contamination and degradation and test the mitigation of such effects, most critically a reduction in the evaporation rate.

Fuel degradation can occur at any point in the supply chain between the refinery and the introduction of the fuel into the device. The degradation can be caused by several factors:

- Chemical reactions between fuel components
- Chemical reactions between fuel components and air
- Chemical reactions enhanced by the surface chemistry of containers or tubing materials
- Chemical reactions between fuel components and container or tubing materials
- Container or tubing material components being dissolved into the fuel liquid

In addition, the fuel can be further degraded within the device unless the device is specifically designed to minimize degradation.

Fuel degradation is detrimental to an evaporator due to the potential for inclusion of low-volatility or non-volatile chemical species at the liquid-vapor boundary. An admixture of low-volatility or non-volatile components in the fuel liquid can result in the deposition of such components at the liquid-vapor boundary. Such deposits can result in inhibition of liquid flow that will degrade the operation of the evaporator, possibly to the point of failure.

The proper design of the evaporator must prevent such degradation from resulting within the useful lifetime of the device. Conversely, if such degradation is unavoidable, designing easy maintenance options, such as replaceable evaporator surfaces, can be done if necessary.

To minimize fuel degradation within the device, the temperature of the fuel liquid should be kept as low as possible to decrease the reaction rate for chemical reactions that can degrade the fuel. This turns out to be readily accomplished and a natural consequence of the stable temperature gradient that becomes established as the dynamic azeotrope takes effect.

The requirement of a stable liquid-vapor boundary with heat applied only to the boundary, however, yields advantages such as:

- producing a minimum possible increase in the temperature of the liquid,
- relative orientation insensitivity, and
- a suitable surface for integration of sensors, mitigation devices, catalysts, etc. This then allows for implementation of practical, commercially viable designs.

Since catalytic combustion requires a fuel vapor-air mixture, rather than pure fuel vapor, there is an additional means of reducing the fuel liquid temperature. Designing the evaporator so that air flows over the fuel-vapor boundary will cause the liquid temperature at the boundary to be less than the temperature that would be required if pure vapor were to be produced, because the presence of the air decreases the partial pressure of the vapor below atmospheric temperature.

The selection of all materials that come into contact with the fuel, such as the reservoir and interconnect tubing, must take into account the degradation processes listed above. In particular, both practical experience as well as literature searches confirm that various metals and polymers are known to cause fuel degradation or contamination and need to be avoided.

If these components have moderately low-volatility, then the boundary temperature will eventually level off to a new equilibrium. If the accumulation consists largely of non-volatiles (e.g., sludge), a continuous temperature increase will result.

The following protocol was used to produce Jet-A degraded by the combination of exposure to air and elevated temperature.

The fuel samples are designated as :

- Fresh: Jet-A Stored for 10 months in polyethylene without exposure to air, light, or elevated temperatures
- Lightly Aged: Jet-A aged in the lab by refluxing for 18 hours at 100 °C and aerated at the concurrently.
- Contaminated: Jet-A purposely contaminated separately with PVC tubing palsticizer and then in another batch with water only.

The plasticizer generally employed in PVC tubing is DEHP (di-2-ethyl hexyl phthalate), which has a boiling point of 385 °C, but which undergoes thermal decomposition in the 180 °C range. DEHP is also highly soluble in hydrocarbon liquids. Since PVC tubing is in widespread use, we examined DEHP contamination. Phthalate plasticizers have been used by some manufacturers in

making so called fuel-tolerant plastic tubing; therefore, it is assumed that this particular plasticizer is representative of the many other phthalate type plasticizers found in a wide variety of plastics and might be encountered in the field.

The second contaminate used was water. In the examples shown below, the water contamination level was set at ~3% by volume. The water was made to be semi-miscible by drop-wise addition over an hour's time at elevated temperatures and with constant stirring. This is a rather high level, and it is felt it would seldom be encountered in practice, but represents an upper bound to fuel that is sitting around in partially filled tanks for long periods where condensation could be present.

During tests with fresh Jet-A and lightly-aged Jet-A, the evaporating surface of the wick was not significantly discolored. Only a slightly yellow stain was noted and appeared have only a small effect on the evaporation rate or dynamic azeotrope.

In contrast to this result, tests run using the extract obtained from exposing PVC tubing to Jet-A shows a wick that rapidly darkened. It eventually turned completely black after only a single test. This can be seen in **Figure 12**.

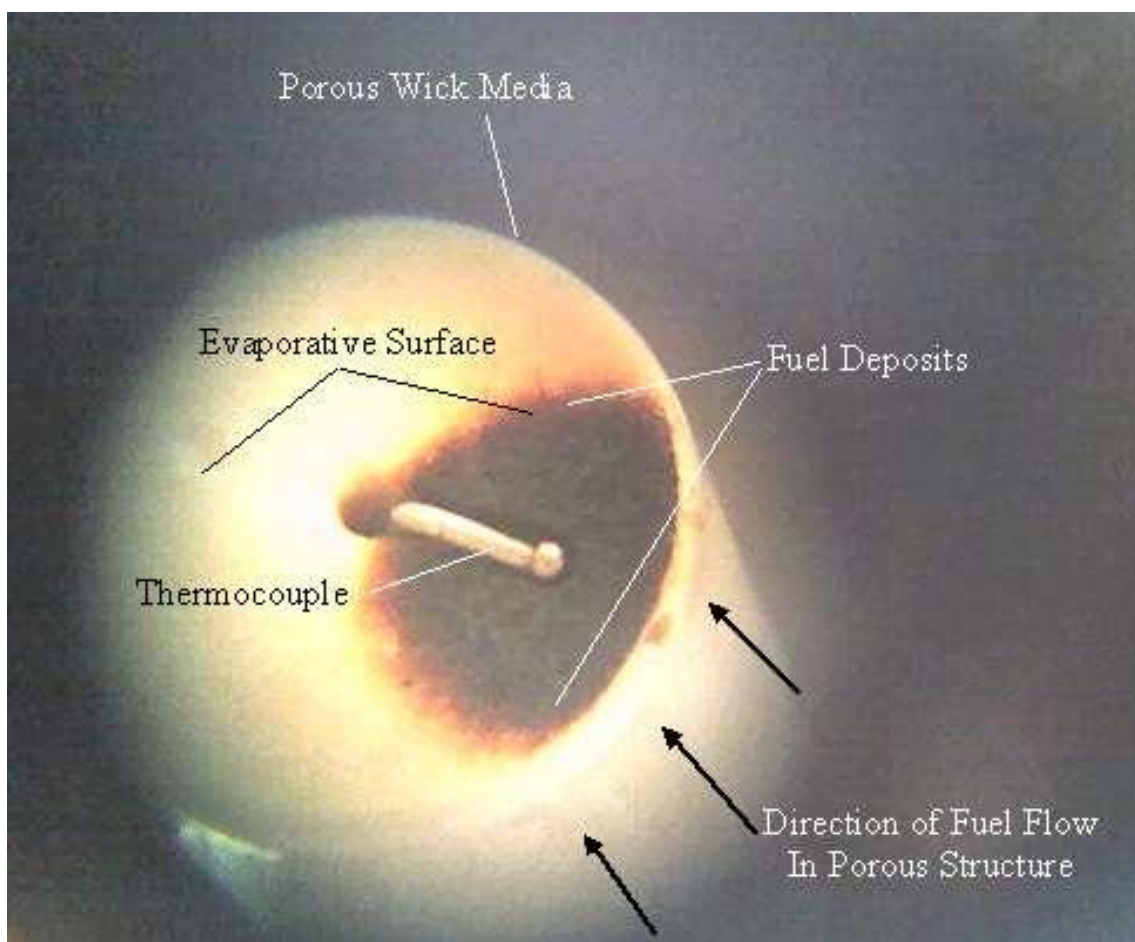


Figure 12. Close-up of Test Surface After Running Contaminated Jet-A

Further testing was done using various combinations of aged and contaminated fuel. The results are recorded in **Figure 13** and **Figure 14**. The left side of **Figure 13** shows the plasticizer causing an increase in the boundary temperature of the evaporator surface. This is interpreted to mean that the azeotrope is breaking down and the fuel/air composition is therefore not stable (i.e., constant in composition over time). The right side of **Figure 13** shows a constant temperature over time and illustrates how a near perfect dynamic azeotrope should appear.

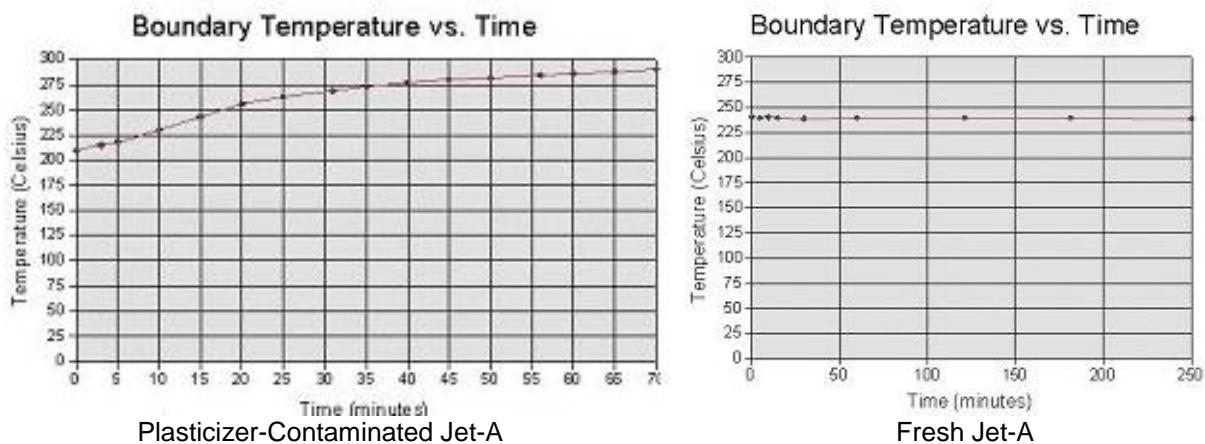


Figure 13. Effect on Azeotrope from Aged & Contaminated Fuel

Figure 14 shows a similar but less pronounced effect of an unstable azeotrope which results from water contaminated fuel. Note that in comparison to the plasticizer contaminate the water contamination is a much smaller temperature change over a much longer period.

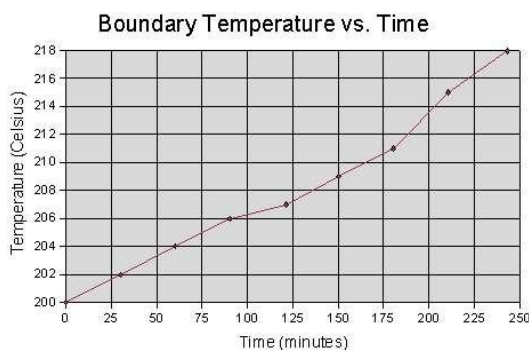


Figure 14. Effect on Azeotrope from Water Contaminated Fuel

It was determined that only the plasticizer (phthalates) contamination mechanism appeared to result in significant deviations from stable evaporation.

These results are interpreted to mean that the dynamic azeotrope technique will work well with any "normal," reasonable quality, jet-fuel.

4.3.7 Vibrating Shutter Nebulizer

The vibrating mesh approach is an alternative approach to providing a metered flow of micro-atomized fuel to a catalytically active surface or reactor. In this method, droplets of fuel are formed by rapid motion of an actuator that creates transient pressure pulses on the liquid surface of the fuel. The surface of the liquid is in contact with a thin sheet of metal that has a multitude of microscopic holes. If the pressure transient is of sufficient magnitude, the liquid is forced through the holes and forms a free droplet traveling away from the surface. A series of droplets are driven out of the microscopic holes during each pressure pulse. Between pulses, the actuator, located below the metal screen, retracts and pulls in fluid from an adjacent reservoir.

Figure 15 illustrates the principle components of such a mechanism and shows the free droplets exiting the metal screen.

The typical orifice size for the metal screen is on the order of 5 microns in diameter separated by a distance of about 100 microns. The resulting spray of droplets is somewhat analogous to the inkjet devices, although, unlike the ink jet, the droplets cannot be made to selectively exit from any particular orifice.

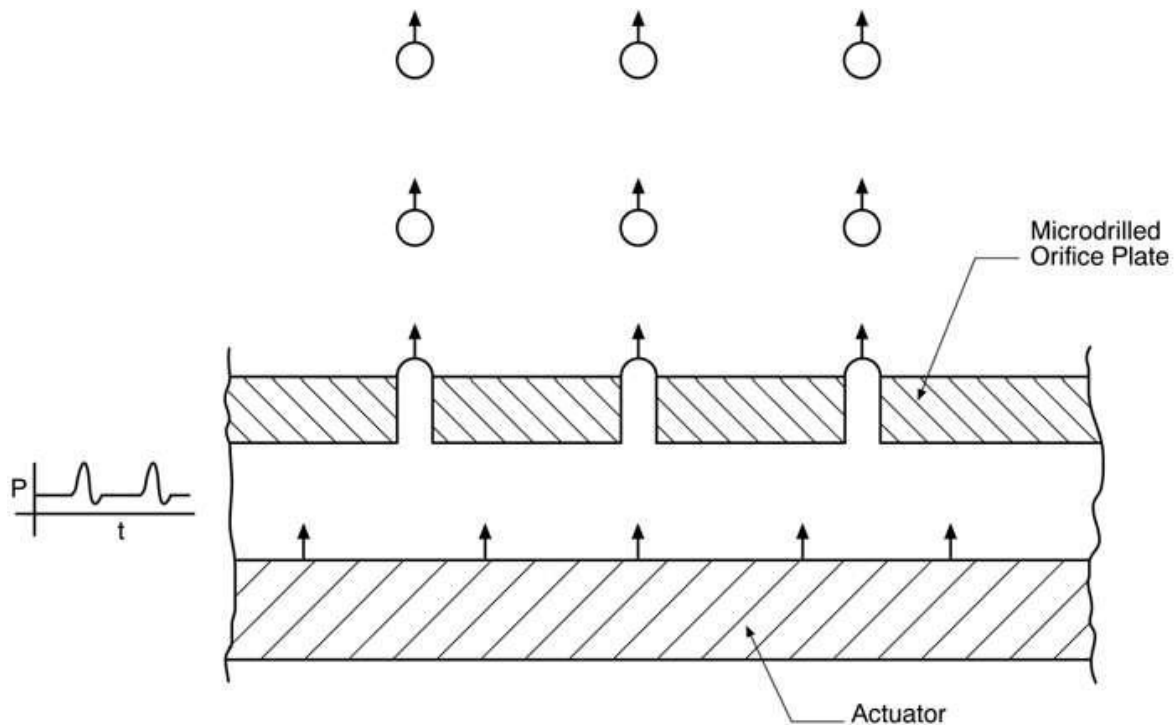


Figure 15. Nebulizer Principle of Operation

An example showing the use of a vibrating mesh nebulizer with both methanol and Jet-A is shown in **Figure 16**. It can be seen on the left that the methanol droplets vaporized quickly after being ejected from the nebulizer mesh plate. This is because of the high volatility property of methanol. The picture on the right shows the vapor trail for Jet-A. The trail is more distinct than the methanol, because Jet-A is much less volatile than methanol; the drops therefore travel relatively long distances in the air before being dispersed by air currents. The Jet-A droplets never actually vaporized at room temperature, but merely drift away from each other until they are no longer visible.



Figure 16. Nebulizer Output Stream with Methanol or Jet-A

For the nebulizer to be a useful fuel metering device for catalytic oxidation reactions, it was necessary to complete the vaporization process. This can be done by including one of several techniques.

One method is to preheat the Jet-A. An alternative approach is to allow the droplets to impact a pre-heated catalytic surface (e.g., electrical pulse), releasing chemical energy, and forcing the catalytic surface to eventually reach a temperature sufficient to complete vaporization of the rest of the droplet stream.

In the latter stage of this project, in concert with the Army technical point of contact, it was determined that a low-risk fuel metering approach should be the focus. This would allow the project to move more rapidly toward a specific application that could be deployed in the remaining contract time period.

To complete the application deployment within the time constraints, the nebulizer became the preferred vaporizer method. Although the dynamic azeotrope technique described earlier has many advantages over the nebulizer, it was not yet in a state of development that would allow for drawing up prototype fabrication designs and thereby provide a lower risk implementation.

Figure 17 illustrates the relative size and form of a typical nebulizer head using the vibrating mesh approach.



Figure 17. View of Nebulizer Head Assembled

5. Prototype Design and Construction

In the last quarter of the development effort, the focus was toward a demonstration unit that would allow the in-field soldier to connect his personal hydration water supply unit to an accessory device that would "instantly" produce an output stream of hot water. The hot water could then be utilized for a variety of beverage or dehydrated foods.

A re-alignment of project goals was achieved through the joint partnering of CDI and Creare. Both the technique for generating heat and the end application were modified to reduce technical risk and improve delivery schedules.

The primary fuel metering component selected was the Creare vibrating mesh nebulizer in conjunction with an electronically-controlled fuel pump. It was decided Creare's experience in constructing and working with this novel fuel metering and atomizing technique (i.e., ultrasonic nebulization) made it a reasonable choice for maintain the development schedule. In addition they provided sub-system integration services.

CDI provided the basic system architecture, heat transfer studies and optimization designs, as well as catalytic combustor plates, electrically-activated catalytic reaction promoter (i.e., the starter), air pump design and construction, water cooled heat exchanger, and selection of the electrically-activated fluid (water) control valve.

Additional aspects of the process, such as conversion of the fuel droplets to a useful heat output (e.g., droplet transport uniformity, vaporization, starting mechanism, etc.), overall architecture required to maintain proper energy balance, and thermo-electrics configuration, were largely driven by CDI's design team. So the project schedule could be met, it was decided toward the end of the project to not integrate the thermo-electrics module into the system.

Most of what was learned in the earlier part of the project was adapted for this stage of the effort, but several new technical challenges arose and required a rapid development of new designs.

The highlights of this design and construction process are presented in the following section.

5.1 Preliminary System Design for the Flow-Through Water Heater

Figure 18 shows the basic system architecture and form and fit design for the flow through catalytic water heater, aka Instant Water Heater. The several views shown in the figure illustrate some of the design constraints examined.

For example, the choice of location of the fuel was carefully considered as it would effect how much the fuel mixture would pre-heat before the nebulizer received the fuel. The selection of where to place the electronics was important, not just from a heat and space perspective, but also driven by the desire to limit the distance to the nebulizer to avoid having the high voltage cable (several hundred volts) cross through or around the fuel source.

The diameter and thickness of the catalytic combustor plate were studied because they effect the pressure drop that the air pump must overcome. Mathematical calculation and experimental efforts were employed to arrive at the best solution.

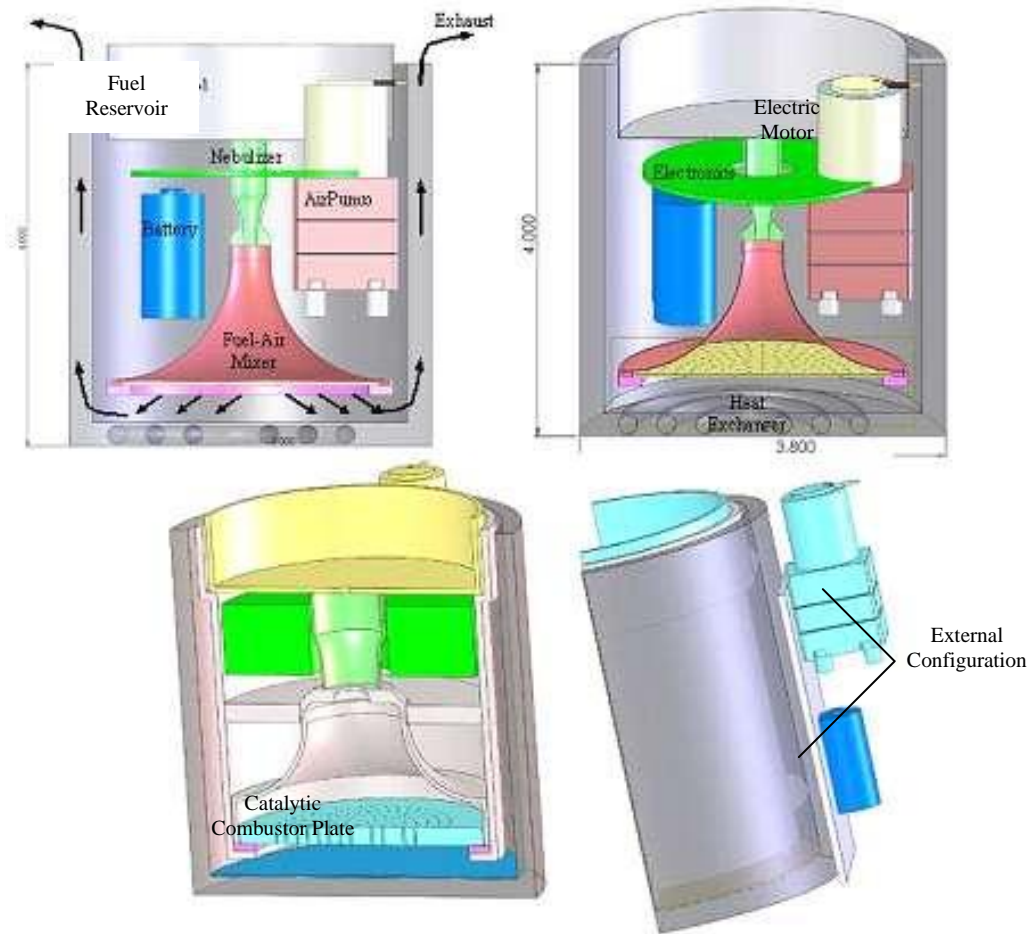


Figure 18. System Design Concepts

If the combustor plate is too large, the pressure drop will be low, but then the surface temperature is reduced -- and thus the radiant energy transfer rate to the heat exchanger. It also causes issues with uniformity of combustion and difficulty with electronic light-off. On the other hand, if the plate is too small, it will overheat the catalyst, causing sintering of the platinum particles and a consequential reduction in power output. These issues were resolved as described in the following sections.

Other trade-off studies were directed toward whether the air pump and battery should be internal or external, optimum distance from the combustor plate and heat exchanger, degree of heat recuperation from the exhaust, size of the fuel tank, method of controlling water flow through the exchanger to avoid vapor-lock (i.e., steam bubbles preventing flow) and proper shut down in case of non-standard conditions (e.g., sudden loss of water supply).

The performance requirement for the IWH is to heat two cups (473 ml) of water from 40 °F to 200 °F, in 10 minutes, under conditions of continuous hot water flow exiting the system.

Using the specific heat-capacity of water (4.184 joules/gram-K), the mass of water (473 grams) and the desired temperature increase ($160\text{ }^{\circ}\text{F} = 89\text{ }^{\circ}\text{C}$), the required amount of heat energy is 176 kilojoules. If uniformly applied over 10 minutes, this amounts to a power level of 293 watts at 100% efficiency.

If a conservative estimate of 60% efficiency is selected, this results in a power level of 488 watts and a total heat energy of 293 kilojoules. Using the lower heating value of Jet-A of 43 kilojoules/gram and the fuel density of 0.81 grams/ml, the mass of fuel required will be 6.8 grams and the volume will be 8.4 ml.

The heater will employ flows of water, air, and fuel. The flow rates for the above quantities over 10 minutes time will be 0.79 ml/sec (47 ml/min) for water and 0.014 ml/sec (0.84 ml/min) for fuel.

For a stoichiometric air/fuel mixture, the required air flow rate will be 148 ml/sec (8.9 liters/min). To provide for complete combustion, we will employ a slightly lean mixture with an equivalence ratio of 0.9, resulting in a required air flow rate of 9.9 liters/min.

Improvements in efficiency will result in a lower fuel requirement as well as a lower air flow rate. 100% efficiency would result in a fuel consumption of 5.0 ml and a required air flow rate of 5.9 liters/min.

5.2 Subsystem Modeling, Design & Testing

The control electronics package was provided by Creare. The original concept arrived at by CDI proposed the following functionality:

- Microcontroller for flow control, startup, and shutdown sequencing
- Temperature sensor inputs
- Liquid sensor inputs (for detection of priming and liquid depletion)
- Pump control voltage outputs
- TEG input (i.e., Thermo-Electric Generator -- later deleted from the deliverable)
- Battery pack and charging circuit

To produce electrical power, a TEG was studied. The TEG could be bonded to the heat-absorbing face of the water heat exchanger in the center of the spiral (described later). This would provide for the lowest possible cold-face temperature for the TEG.

The cold water enters in the center of the heat exchanger (HX) so as to ensure the hot face will not exceed operational limits. TEG's from Hi-Z are designed to operate with a thermal power flux of 10 watts/cm^2 , and this matches well with the calculated radiative power flux from the catalytic combustor plate. The TEG could be sandwiched between a pair of aluminum plates to act as heat spreaders and mounting interfaces, as shown in **Figure 19**.

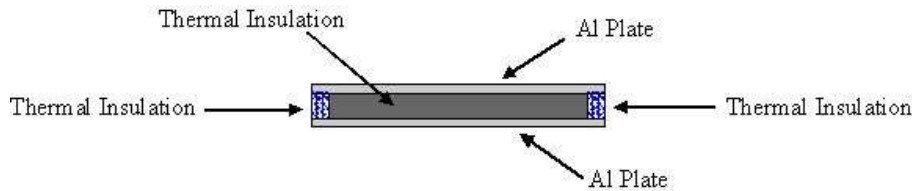


Figure 19. Placement of TEG in Heat Flow Path

In the course of the design effort, it was determined the TEG subsystem would add an additional two months to the project and was deleted as a near term goal in order to maintain schedule.

The air pump design was decided to be a radial-vane pump engineered and produced by CDI. The water metering device was self-priming and consisted of a solenoid activated valve. The valve was placed up-stream of the water cooled heat exchanger. The siphon effect enabled the use of only one valve placed at the inlet to the heat exchanger.

The siphon effect prevented water from flowing through the heat exchanger during the "off" condition. To regulate water temperature, the valve was conceived with an idea that it could be turned on and off in a manner such that the duty cycle could be actively altered by the electronics and the average net flow-rate controlled as desired.

5.2.1 Catalytic Combustor & Heat Exchanger Subsystem

A computational study of the heat transfer mechanism was performed to provide a determination of relative efficiency and the basic physical properties of the unit. The goal was to find a design that allowed a rugged, compact, lightweight, readily manufacturable topology while allowing the water to reach appropriate exit temperatures at specified flow rates.

The task was divided into four milestones:

- (a) Advanced computational fluid dynamics (CFD) modeling experiments were performed to assess basic theoretical feasibility of the design.
- (b) Preliminary conceptual design for an integrated assembly containing (1) the radiant/hot gas absorber surface, (2) heat diffuser plate, and (3) fluid conduit layer water loop
- (c) Assembly of a proof-of-concept heat transfer package
- (d) A water flow rate controller and test set-up

Figure 20 and **Figure 21** illustrate a result of milestone (a). They show the outcome of asking a hypothetical question and answering it through CosmosFlowWorks, a CFD software program.

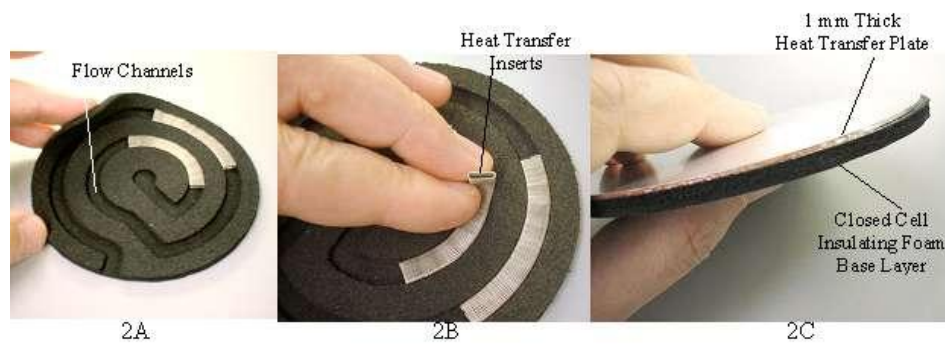


Figure 20. Inside Views of High Performance Heat Transfer Unit



Figure 21. Top and Bottom Views of Heat Transfer Unit

The hypothetical question was: What fluid path length would be required for the water to arrive at a temperature equal to the average receptor plate temperature before exiting? Implicit to this question are parameters such as flow rate, flow channel material properties, flow channel dimensions and patterns.

To maintain a low weight and to provide for a simple and cheap manufacturing approach, it was decided to use as much low-density polymer material in the construction as feasible. In practice, making the whole serpentine path out of aluminum is possible, but not practical, because of expense and weight, and also because the thermal mass of the whole heat transfer unit becomes problematic. For instance, if the fluid is suddenly stopped, a large excess of thermal energy will drain into the stationary water and could raise its temperature above boiling. To make the unit safe using a solid metal mass might require special design and extra unit cost.

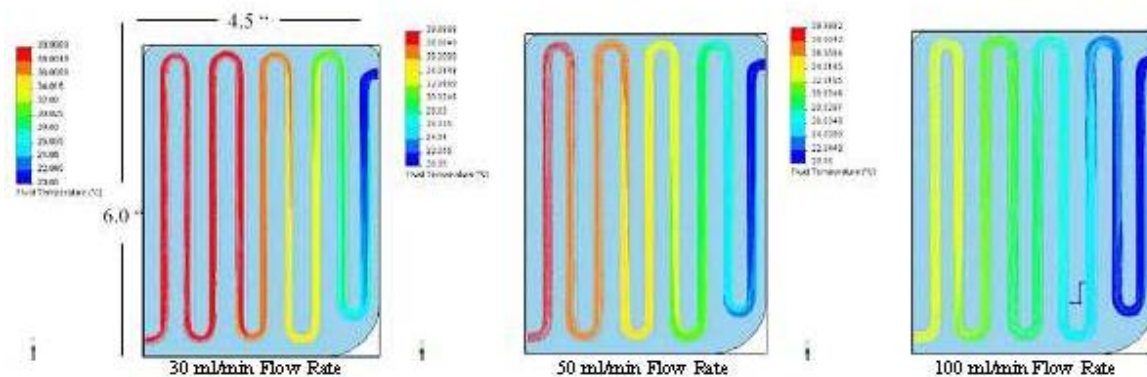
To this end, it was decided the heat exchanger would consist of three parts. The first part is a thin metal heat receptor which intercepts and absorbs the radiant heat energy (and some hot gas transfer as well) emitted from the glowing catalytic combustor plate.

Because the receptor plate temperature is monitored to prevent overheat and thus a system shut down can be implemented instantly, it was reasonable to build the remaining portion of the heat exchanger out of lightweight polymers. The metal receptor plate also acts to keep the low temperature materials in the shadow of the radiant heat emission, preventing direct exposure to temperatures exceeding the materials relatively low temperature-rating (i.e., 325 °F).

Figure 22 shows the result; in order for the water to reach equilibrium with the receptor temperature before exiting into the beverage cup, it is necessary for the fluid path to be on the order of 50 inches in length for a flow rate of 50 ml/minute. The boundary conditions associated with Figure 22 are that the water experiences heat flow through only one side of the channel; that is, heat flow to the water through the metal wall of the receptor plate and not from the walls of the polymer base layer.

Heat Transfer Study

Illustration of Water Flowing Over A Fixed Temperature (i.e.40°C) Aluminum Plate
Without Embedded Metal Inserts in Fluid Channels



NOTE: Path length of water is 50 inches

Fluid temperature Along 50 inch Serpentine Path

Figure 22. Example of Poor Heat Transfer Design

Figure 23 shows that the fluid path length, required to reach equilibrium with the receptor plate temperature, can be easily dropped to half the former path length (i.e., 25 inches) if a metal insert is included within the channel structure. As was seen in Figure 20, the insert chosen was custom-made in the form of a rectangular stainless-steel spring.

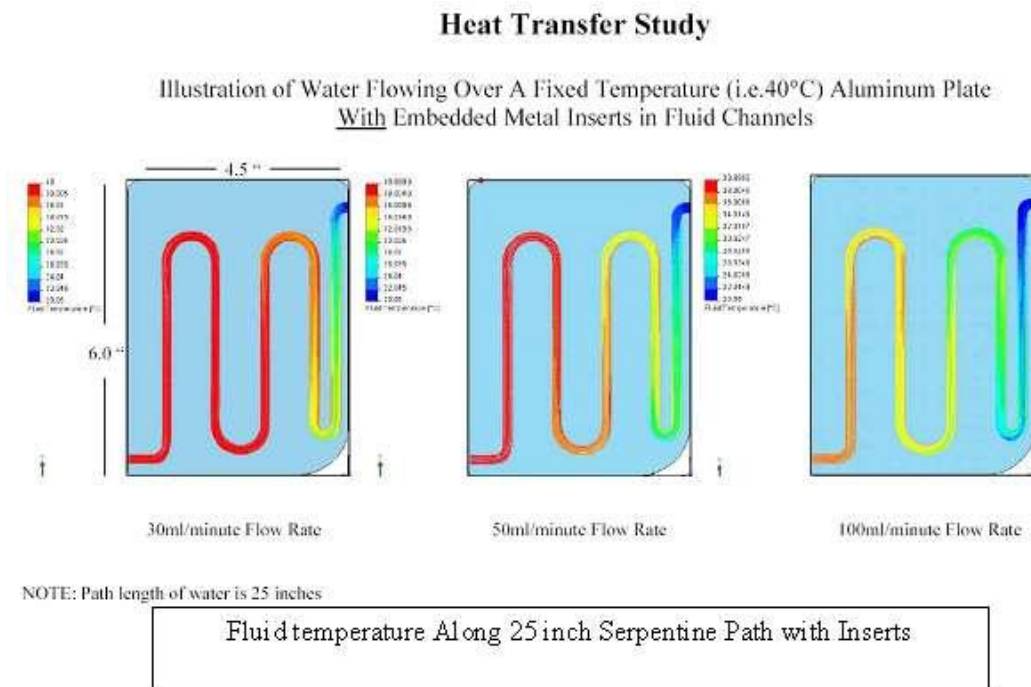


Figure 23. Significantly Improved Heat Transfer

Performance data for the completed unit, as illustrated in these figures was gathered using an electrically regulated film heater bonded to the receptor plate. The results from this testing are displayed in **Table 2**.

Table 2. Heat Exchanger (HX) Test Results

	Test #1	Test #2	Test #3	Test #4
Inlet Temperature	20°C	20°C	20°C	20°C
Outlet Temperature	38°C	61°C	78°C	96°C
Water Flow Rate	50ml/minute	50ml/minute	50ml/minute	50ml/minute
Plate Temperature	50°C	75°C	100°C	120°C

Four separate test criteria were run to establish a range of performance. Each test consisted of fixing the receptor plate temperature and then flowing the water through at a constant rate of 50 ml/minute. The resulting water temperature at the exit was recorded. In this case, the fluid path was by necessity less than the ideal length of 25 inches -- it was in fact set to 12 inches.

However, it can be seen from the result that the degree of over-temperature required of the receptor plate to force the exit temperature of the water to near boiling is relatively minor. The primary reason for the shorter than ideal path length was simply that the metal insert was designed before the ideal path length was confirmed through modeling; therefore, the channel widths were fixed to match the insert width. In the future, reducing the channel width and metal insert width by half will result in a full 25 inches within the same device size, improving heat transfer efficiency.

Figure 24 shows the same heat exchanger data. It is indicating that the water temperature reaches roughly 80% of the receptor plate temperature before exiting.

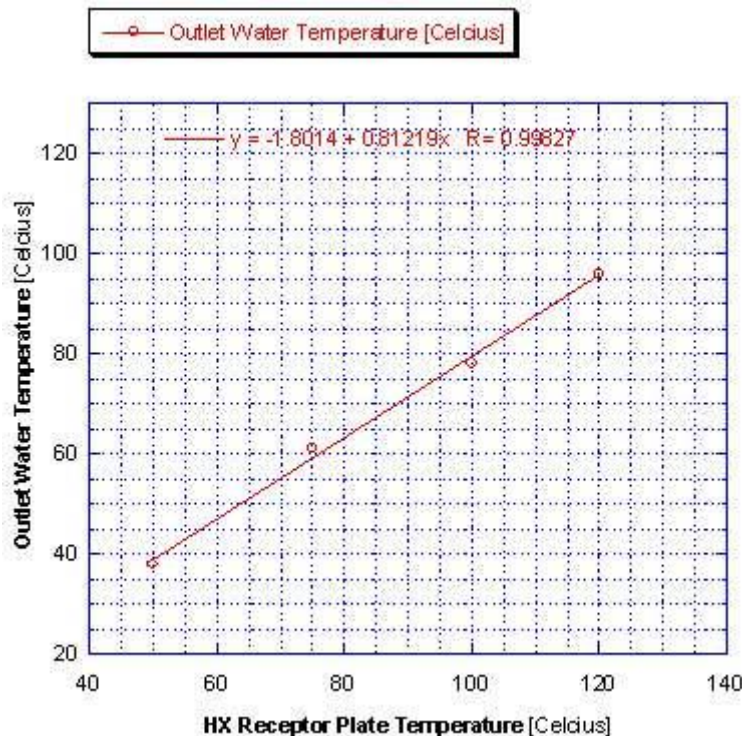


Figure 24. Advanced Heat Transfer Prototype Performance

The intent of the design was to allow for a low enough pressure drop across the HX unit so that even very low pressure heads, such as encountered in gravity fed system like a personal hydration unit, will give at least 50 ml/minute of flow rate.

Figure 25 illustrates that the water pressure drop occurring in the heat exchanger is sufficiently small to allow gravitationally motivated head pressure of the hydration unit to drive the system at 50 ml/minute or greater.

The performance will allow for a range of flows from 0–100 ml/minute. This allows the water flow-rate parameter to be used as the controlling variable for water exit-temperature. By electronically adjusting the average flow rate, water temperature is then easily regulated even though the heat combustion power is fixed at a constant value.

The results shown in Figure 25 are a trade-off between pressure drop and heat transfer effectiveness (not efficiency). This is because the CFD models demonstrate that the fluid comes to equilibrium with the receptor plate temperature only if the path length is maintained above a certain critical value. However, a longer path length increases pressure drop and requires a greater pressure head to achieve the same flow rate.

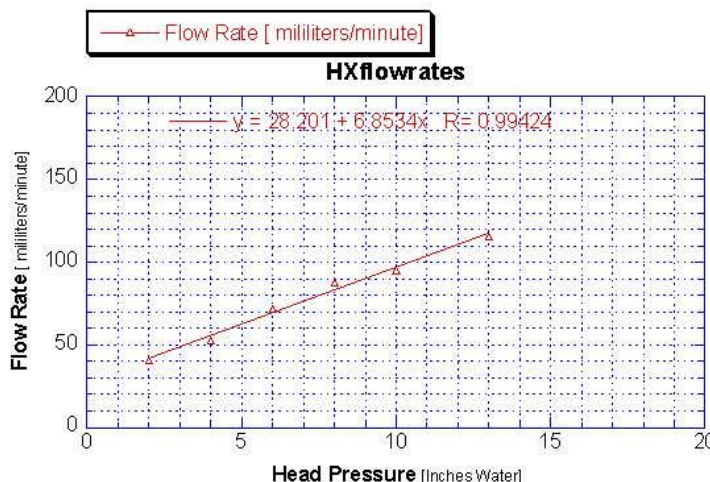


Figure 25. Pressure Drop versus Flow Rate

5.2.2 Catalytic Combustion Chamber

One of the primary challenges in catalytic combustion is to provide adequate heat transfer from the combustor plate to the water HX receptor plate, in such a way that the following requirements are met:

- (a) The combustor temperature is kept high enough to perform fuel droplet vaporization without leaving deleterious deposits.
- (b) The combustor temperature is kept high enough to perform complete catalytic combustion of the fuel.
- (c) The combustor temperature is not so high that it degrades the catalyst.
- (d) The temperature range conforms with items (a) through (c) throughout power variations required during startup, operation, and shutdown.
- (e) The effective thermal mass of the combustor, and all materials with which it is in thermal contact, remains low enough that only a reasonable amount of energy is required to heat it to ignition temperature.

It can be shown that an adiabatic catalytic combustor running at a very lean equivalence ratio of 0.4 and using a conventional heat exchanger to transfer heat from the catalyst exhaust gas to the water could achieve the above goals.

For an adiabatic design, the catalyst temperature would be equal to the adiabatic flame temperature associated with a particular equivalence ratio. It would also be independent of power output level over (in principle) an arbitrarily large power range.

In addition, since the heat would be carried from the combustor to the water heat exchanger via the flow of the hot gases, the catalyst would not need to be in conductive contact with any other part of the system, save for the requirements of mounting.

The adiabatic reactor design, unfortunately, does not provide for the possibility of the small form factor desired for the IWH application; however, it is possible to modify the design in a manner that will allow for a small planar form factor.

This can be done by using thermal radiation, in addition to convection, in order to transfer heat from the combustor to the water heat exchanger. Since the catalytic combustor can operate at temperatures of many hundreds of degrees Celsius, the radiant heat generated by a reasonable surface area (a 3" disc) would fulfill the design goals of the IWH. This was explored in detail using a CFD model discussed in section 5.2.3.

To be specific, for a temperature of 900 °C the heat radiated per unit area is 487 watts. Due to the very steep dependence of radiant heat flux on temperature (T^4), a relatively large change in the power generated by the combustor would result in a small temperature change. For example, doubling the power output would increase the (Kelvin) temperature by a factor of the fourth root of two -- a 19% increase.

We see from **Figure 26** that the adiabatic combustor exhaust temperature for a stoichiometric mixture ($\Phi=1$) is about 2100 °C -- much too high for any catalyst or support. However, a

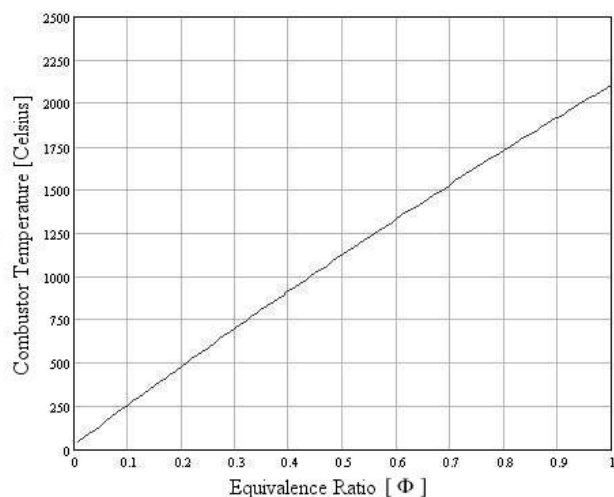


Figure 26. Combustor Temperature vs. Equivalence Ratio

mixture with twice the air required for a stoichiometric mixture ($\Phi=0.5$) produces a combustor exhaust temperature of 1100 °C, and ten times stoichiometric air yields only 250 °C -- the latter being within the range of some flexible polymeric materials, although this would require a much higher-volume air pump. More practically, an equivalence ratio of 0.3 produces a temperature of

700 °C, which is low enough so as to not degrade the catalyst, but high enough to oxidize any deposits of carbonaceous material in the catalytic combustor (as may occur if a fuel nebulizer is used).

To achieve the above design goals each subsystem must be examined in terms of their interaction with other parts of the whole system and not just as individual components. These subsystem components are given a preliminary assessment below.

For the combustion to be uniform within the catalytic reactor, which is required so as to ensure uniformity of the combustor temperature, the aerosol and air flows must be uniformly mixed. And to minimize the volume of the mixer, the design envisions a cylindrical swirl-mixer with a diameter of 1" and a length of 1".

The aerosol will be injected along the axis of the cylinder and the air will be injected along the wall of the cylindrical chamber, perpendicular to the axis and tangential to the wall, as can be seen in **Figure 27**.

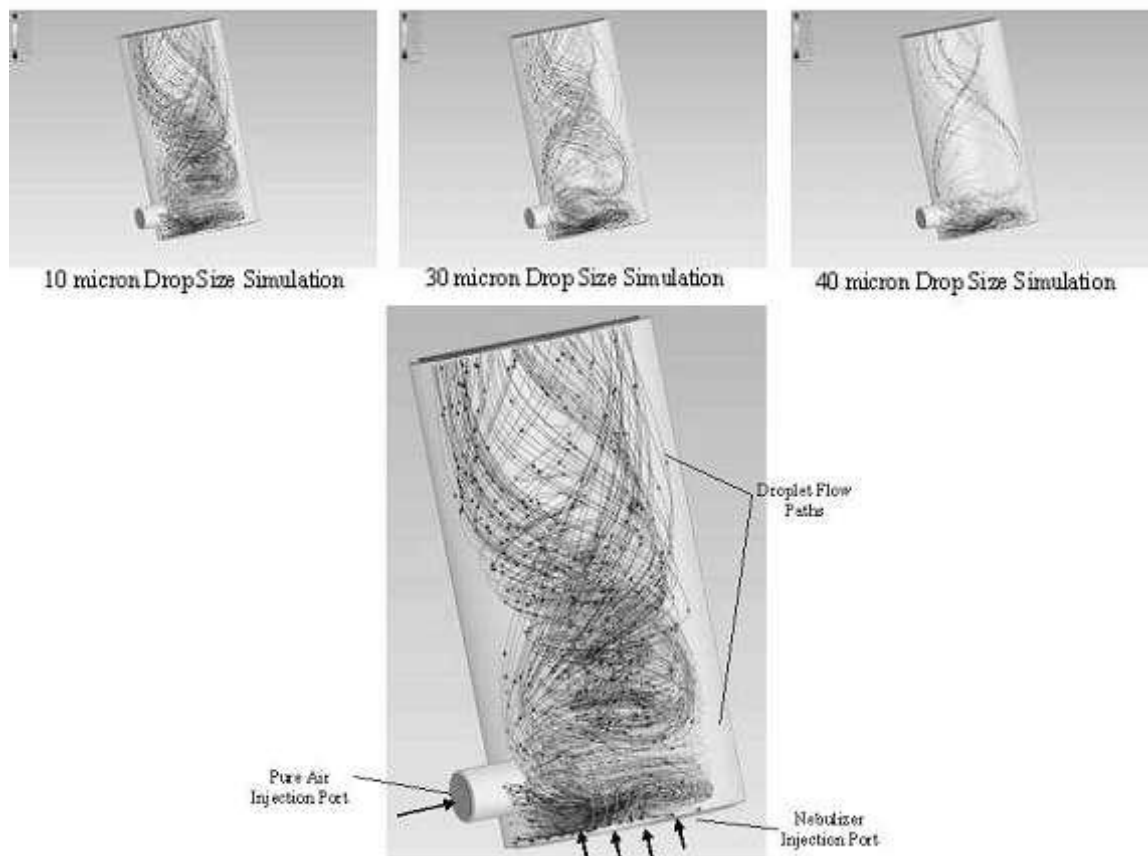


Figure 27. Visualization of Fuel Droplet Size vs. Transport Effectiveness

The rotating flow pattern of the air will subject the fuel droplets to a large centrifugal force and distribute them outward toward the cylinder wall. The diameter of the air injection port was adjusted in order to achieve adequate uniformity of mixing without causing impingement of the droplets on the cylinder wall.

CDI has run several Computational Fluid Dynamics (CFD) models. They are shown sequentially in terms of droplet size along the top of Figure 27. The model suggests that the droplet size emitted from the Creare nebulizer has a critical effect on the mixing process, as would be expected from first principals.

More specifically, the model shows that when the nebulizer injects droplet diameters above 10 micron in size, it can be expected that a portion of the aerosol will make contact with the walls of the mixing vessel.

The top row of images in Figure 27 show the result of droplet size increasing from left to right, spanning a range from 10–40 microns.

The CFD model was programmed to terminate the flow-stream paths at the point where the droplet touches a wall. Thus, in going from 10 micron to 40 micron drop size, the result is that the number of paths making the complete journey through the mixer without impacting a surface are seen to drop off significantly.

The importance of the increasing impingement is that condensation of the fuel is likely to result in the mixing area; consequently, reduction of the system power output and a pooling of condensed fuel over time may result. The 10-micron drop-size recorded by Creare for their nebulizer is the peak value expected. Since the droplet size distribution is not a mono-chromatic distribution, droplets of greater diameter are expected.

The problem will have varying significance depending on the design. If the wall of the chamber is coated black, the absorbed radiant heat from the glowing combustor plate may be able to partially ameliorate the problem. This would favor a set-up where the nebulizer fuel injection rate and air-flow rate are constant. In this way the inner wall of the chamber can then be tuned to receive the optimum amount of feedback radiant energy. **Figure 28** shows the actual interior of the combustion chamber and the catalytic combustion plate during a JP-8 fuel test operation.



Figure 28. Test Bed for Nebulizer-Based Catalytic Combustion

Alternatively, since the combustion plate, after reaching equilibrium temperature, will be of a temperature to instantly vaporize any fuel condensate, then the inner wall of the chamber could be redesigned mechanically so the condensate does not escape out the edge of the plate. This would require machining a special interior lip near the exit of the chamber to redirect any condensate toward the center of the combustion plate.

Figure 29 illustrates two possible sources of air for the system. The photo on the right shows a high efficiency, high flow, rotary vane air pump designed and constructed at CDI. While it is able to easily handle the pressure drops likely to be encountered in forcing air through the catalytic combustor plate, it is nevertheless bulkier, heavier and more power consumptive than would be desired in an actual product. Calculations have shown that the utilization of low back-pressure metal foam combustor plates (instead of porous ceramic) along with some re-design of the input ports of the mixing chamber could in theory allow the use of micro-blower assemblies.

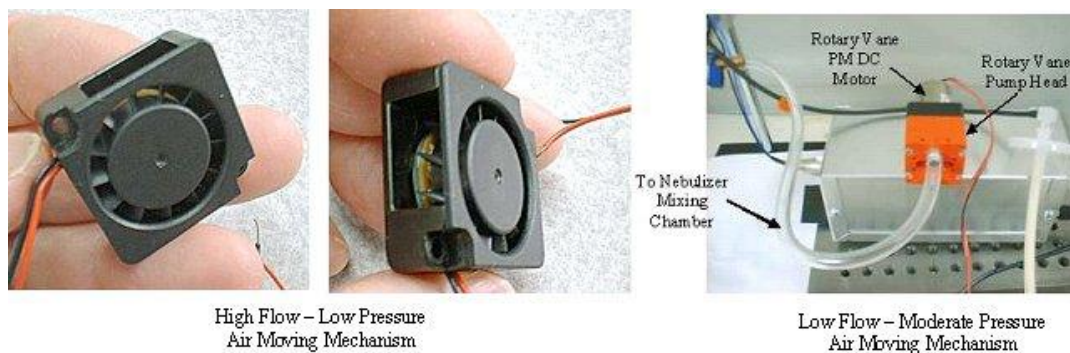


Figure 29. Alternative Air Moving Mechanisms Evaluated

The micro-blower generally has a comparatively high flow-rate with respect to the same sized rotary vane pump but "pays" for this improved flow rate by limiting the pressure drop capacity to under 1" of water.

The two left photographs in Figure 29 show an example of one possible micro-blower to be considered in future work. It is a brushless-motor driven device with integral pole switching and sensing circuitry built into the blower body. Because it is brushless, the lifetime is expected to be in the many thousands of hours.

In addition, this particular blower model claims to have a maximum pressure drop capability of 0.36 inches of water pressure. If this is true, it may be possible to obtain the required 6 liters per minute flow rate (and above) with minimal battery power (e.g., less than 0.125 watt) with very low weight and noise.

The blower does not come with a shroud or ducting, and this will need to be specially designed and coupled to the mixing chamber. Also, the input port to the mixing chamber will need to be modified to accept this device so as not to place any addition pressure drop in the path of the blower.

5.2.3 Gas Flow and Heat Transfer Calculations

An important concern in the design of this application has to do with keeping operational parameters within certain bounds to avoid adverse effects. Some possible adverse effects include sintering of the catalyst, flashback of the fuel-air stream, insufficient radiative energy, insufficient vaporization of droplets at the combustor plate, and excessive pressure drop across the combustor plate. Initially, a series of first order manual calculations were performed to help direct the design effort.

To simplify the analysis, a geometry was used that is disposed to both experimental investigation and theoretical analysis. The model geometry comprises a 1"-diameter porous disc affixed to the end of a 1"-diameter Pyrex tube. The geometry is shown diagrammatically in **Figure 30**.

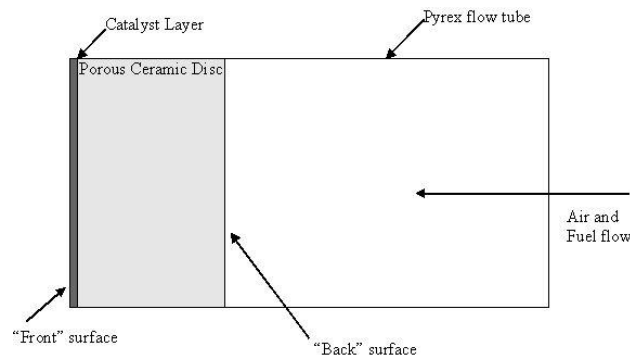


Figure 30. Model Geometry for Gas & Heat Flow Estimates

To estimate certain critical parameters of operation, a thermal profile calculation was performed of the flow as it (a) travels through the flow tube to the porous ceramic disc, then (b) through the disc (profile view). From the latter we can then calculate the pressure profile, which will be vital in determining the selection of porous material and the performance needed from the air pump.

The following calculations were performed with a porous alumina material in mind to be used as the combustion plate structure. Later, an alternative material, made from a stainless-steel metal foam would ultimately be found to be a better choice. Nevertheless, the process presented here for assessing performance is the same.

A few simplifying assumptions were made in order to carry out the calculation analytically:

- We will ignore the fuel aerosol component of the flow. This component occupies a total volume more than three orders of magnitude smaller than the air volume, this simplification will not noticeably affect the result.
- We will assume that the flow is laminar. The Reynolds number for the air flow in the tube is about 30, small enough for the flow to be laminar if no vorticity is intentionally introduced. In the actual device being designed there is considerable vorticity introduced by the swirl mixer, so the extension of results in this calculation to the actual device was carefully considered.
- Air entering the porous disc immediately takes on the temperature of the back surface of the disc by assuming that the thermal entry length is zero. The actual thermal entry length is small compared to the other dimensions of the geometry. In particular, the flow

velocity into the disc is very small (about 2 cm/sec) and the pore size of the ceramic disc is also very small (about 20 μm).

- We ignore the effects of buoyancy on the heated air. This allows for a further assumption that the air flow is entirely one-dimensional, accurate to the extent that the zone of heated air near the back surface of the disc is very thin -- which the calculation will reveal.

The temperature of the air as a function of distance from the back surface of the porous disc was calculated based on the assumption that the flow is entirely one-dimensional and the air is at the same temperature as the back surface of the disc at the point at which it enters the disc.

This is a problem in combined conduction and convection, with heat being conducted by the air away from the surface upstream and heat being carried by the flow towards the surface downstream. Therefore, the time-dependent heat diffusion equation was used. For the one-dimensional case, it is as follows:

$$\frac{\partial T}{\partial t} + V * \frac{\partial T}{\partial x} = \alpha * \frac{\partial^2 T}{\partial x^2} \quad (2)$$

where T is the temperature, x is the distance from the back face of the disc, and α is the thermal diffusivity of air. Since we are looking for a steady-state solution, the time derivative vanishes and the equation becomes an ordinary second order linear differential equation:

$$\frac{d^2 T}{dx^2} - \left(\frac{V}{\alpha}\right) * \frac{dT}{dx} = 0 \quad (3)$$

Where V = flow velocity, the solution to which is:

$$T(x) = C_1 * e^{-x/x_0} + C_2 \quad (4)$$

where the C_i are constants of integration, and $x = \alpha/V$

When the boundary condition for x is set to infinity, T equals the input air temperature, which tells us that $C_2 = T_i$ (the initial air temperature). Given that the temperature at $x=0$ is equal to the (as yet unknown) temperature of the back face of the porous disc T_B , we see that $C_1 = T_B - T_i$, so the solution is:

$$T(x) = (T_B - T_i) e^{-x/x_0} + T_i \quad (5)$$

The exponential factor x_0 is, therefore, the distance from the back surface of the porous disk at which the incoming air is heated to $1/e$ of the temperature of that surface or, equivalently, the heat diffusion length.

The relevant values of T_i , T_B , and x_0 are: 20 °C, 500 °C (a desirable value), and 3.9 mm. The thermal profile in the flow tube is shown in the graph in **Figure 31**, with the distance x in mm.

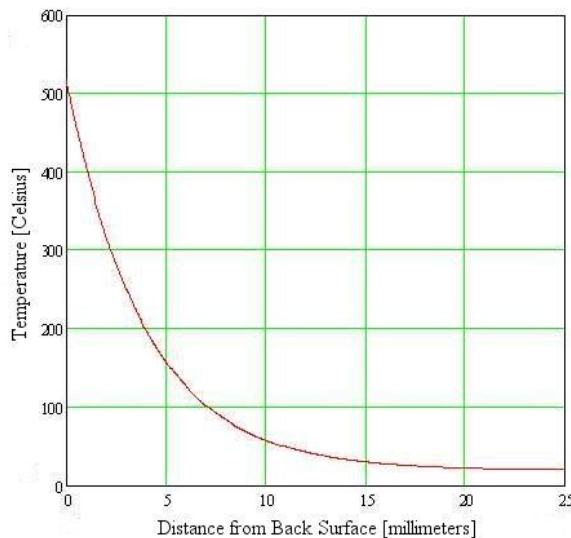


Figure 31. Flow Tube Thermal Profile

Most interesting is the $1/e$ thickness (the heat diffusion length) of the heated layer adjacent to the back face of the porous disc, i.e., near $x=0$. Flashback may occur if the thickness of the heated layer exceeds the laminar flame thickness, which is in the range of several millimeters. Since x_0 is about 4 mm, there may indeed be a flashback problem, at least absent any of the mitigating factors identified below in the section on flashback. However, operation of the prototype so far, have shown that with this approximate model geometry combined with use of the Creare nebulizer and air flow rates (discussed later), that flash back is not observed.

5.2.4 Flashback Analysis

The design of the system requires that the fuel-air mixture not ignite into a flame, but instead oxidize catalytically. The auto-ignition temperature of mixtures of Jet-A vapor and air is 260 °C and the laminar flame velocity is in the range of 30–40 cm/sec. Since the flow velocity of the fuel-air mixture will be only a few cm/sec and the auto-ignition temperature is low relative to the temperature desired for the back surface of the porous disc, flashback must be considered a real possibility.

There are, however, reasons to expect that flashback will not occur in this design:

- The fuel is in the form of an aerosol, not vapor, and it may be that either flame velocity or auto-ignition is inhibited in this case. A literature search has given conflicting information.

- Flashback was not observed with Creare's aerosol-driven stove, even though the flame holder was red hot on the inner surface.
- CDI has experience with kerosene burner systems that do not exhibit flashback unless the fuel-air velocity is decreased significantly (e.g., during shutdown). This may be due to heat from the flame holder being able to diffuse farther back into the fuel-air flow at low velocities and thereby heat a thicker layer.

In section 5.2.3, the thickness of the layer of hot fuel-air adjacent to the hot back surface of the porous ceramic catalyst disc was calculated. It may be a necessary condition that this layer be thicker than the laminar flame thickness, perhaps by several millimeters, in order for ignition to occur. Perhaps a combination of these factors ultimately provided the needed protection against flash back.

5.2.5 Temperature Profile Inside Ceramic Combustor Plate

As with the flow tube model calculation, some simplifying assumptions are used to carry out the calculation analytically. They are:

- The fuel aerosol is immediately vaporized upon entry into the porous material.
- We ignore the fuel component of the flow. As this component, even as vapor, occupies a total volume more than one order of magnitude smaller than the air volume, this simplification will not noticeably affect the result.
- We will assume that the flow is laminar. The Reynolds number for the air flow inside the porous material is literally microscopic so the flow is strictly laminar.
- When the air flows through the porous disc it takes on the temperature of the solid phase of the material. The justification for this assumption is similar to the assumption of a thermal entry length of zero in the previous section.
- The fuel-air mixture is catalytically combusted exactly at the front (exhaust) surface of the porous plate.

The temperature of the air is calculated as a function of distance from the front surface of the porous disc. The flow is viewed as entirely one-dimensional and all of the air is at the same temperature as the front surface of the disc where it exits the disc.

The calculation of the heat diffusion length x_0 , for the air within the porous material, is performed for the case of a disc 3 mm thick, made from Zircar ZAL45-AA. This is a material that has been used to successfully fabricate previous catalytic combustors. The material has a thermal conductivity of 0.22 watts/meter-Kelvin in the 600 °C temperature range, and so the diffusion length, x_0 , for the design flow rate is 15 mm.

Since this is many times larger than the expected thickness for the porous disc, the effects of conduction will dominate convection. Heat will be produced at the front face of the disc, and a portion will be conducted to the back surface where it will be absorbed by the following mechanisms:

- (a) Heating the incoming cold air up to the temperature of the back surface, T_B
- (b) Vaporizing the fuel droplets
- (c) Radiating heat back into the fuel-air mixing and flow chambers

Mechanisms (a) and (b) are vital to the proper function of the heater. Mechanism (c) may be useful to heat the walls of the chamber so that fuel will not condense there, but should be low enough so that the fuel nebulizer is not heated significantly. Radiation can be minimized by ensuring that the emissivity of the back surface of the porous plate is low.

The following calculations help to determine the amount of heat power lost to air heating and fuel vaporization, and will also calculate the amount of radiant heat expected from the back surface.

We will assume that the back surface is at 500 °C, which is a temperature that should ensure that the surface remains free of fuel residue. The heat power required to increase the temperature of the 6 liter/minute flow (i.e., value selected to produce 340 watts of combustion power) is therefore:

$$P_{air} = C_p^{air} * \left(\frac{dM^{air}}{dt} \right) = 62 \text{ watts} \quad (6)$$

Where C_p is the specific heat of air at constant pressure and dM/dt is the mass flow rate of air per unit area.

The heat power required to vaporize the fuel flowing at a rate of 0.6 ml/minute is:

$$P_{vapor} = C_p^{JP8} * \left(\frac{dM^{air}}{dt} \right) = 2.3 \text{ watts} \quad (7)$$

This value is so low that it will be disregarded in subsequent calculations.

The heat power radiated from the back surface at 500 °C, assuming an emissivity of $\epsilon = 0.15$ for the alumina fiber material, is:

$$P_{radiate} = \epsilon_{back} * \sigma * T^4 * A = 15 \text{ watts} \quad (8)$$

The total heat power that must be conducted to the back surface of the porous disc is, therefore, approximately 100 watts, the majority of which will flow back into the disc as heated air.

The Fourier heat conduction formula was used to calculate the thickness of the candidate material, Zircar ZAL45-AA, necessary to provide the conduction of 77 watts from the front to the back surface of the porous disc. This assumes that the temperatures of the front and back are 700°C and 500°C, respectively:

$$t_{disc} = \kappa * A * \frac{\Delta T}{P_{total}} = 3.0 \text{ mm} \quad (9)$$

This is a value that is in the lower range of thicknesses that will provide sufficient strength but should be acceptable.

5.2.6 Catalytic Combustion Plate Surface Temperature

Heat exits the front face of the porous ceramic disc via two mechanisms, radiation and the heat contained in the hot exhaust gases. In this section we will calculate the amount of heat transferred by these two mechanisms, and thereby calculate the temperature of the front face.

The total radiant heat emitted from the front surface is:

$$P_{radiate} = \varepsilon_{front} * \sigma * T^4 * A \quad \left(\frac{1}{0} \right)$$

Since we want to maximize the amount of radiant heat emitted we will set $\varepsilon = 1$ in the following.

The total heat carried from the front surface by the exhaust gases is:

$$P_{exhaust} = C_p^{exhaust} * (T_{exhaust} - T_{reference}) * \frac{dM_{exhaust}}{dt} \quad \left(\frac{1}{1} \right)$$

T_{ref} is the reference temperature that is used to define the enthalpy of combustion (lower heating value) of JP-8, and equals 150 °C. These two powers should add up to the total power. The solution to this quartic equation is solved numerically by setting the total power to 340 watts for this example. The result is that T_{front} is 709 °C.

This turns out to be an acceptable value in that the catalyst will not be caused to deteriorate due to sintering, nor will the alumina be caused to change phase.

5.2.7 Catalytic Combustion Plate Physical Properties

Figure 32 shows a 4mm thick porous alumina (Zircar ZAL-45) disc 2.5 inches in diameter.



Figure 32. Porous Ceramic Catalytic Combustion Plate Substrate

A wide variety of porous ceramic material exist to choose from, so a number of materials were tested for critical properties to determine if they are suitable for inclusion into the design. Both strength, machinability (or formability), thermal conductivity and porosity were evaluated.

Zal-45 was found to be sufficiently strong to stand up to handling required for prototype assembly. It also had good machinability and thermal conductivity, and was stable at temperatures expected to be reached during processing and operation.

Another key property is that the porosity should be sufficient to minimize pressure drop of the air stream. This is critical, because the air pump was chosen to be of a miniature radial vane type running from battery power and has very limited over-pressure capability.

The air pump chosen for the water heater project can produce the required flow rate if the pressure drop is less than 5" of water (about 0.2 psi). The permeability of the porous material must therefore be high enough to ensure that the back-pressure is at or under this value.

Experiments were carried out on three materials from Zircar: ZAL15-AA, AL30-AA, and ZAL45-AA to determine the pressure drop properties of each. For each material, a thin disc was cemented into one end of a Pyrex tube, and compressed air at a known flow rate was pumped into the open end. The experimental apparatus is shown diagrammatically in **Figure 33**.

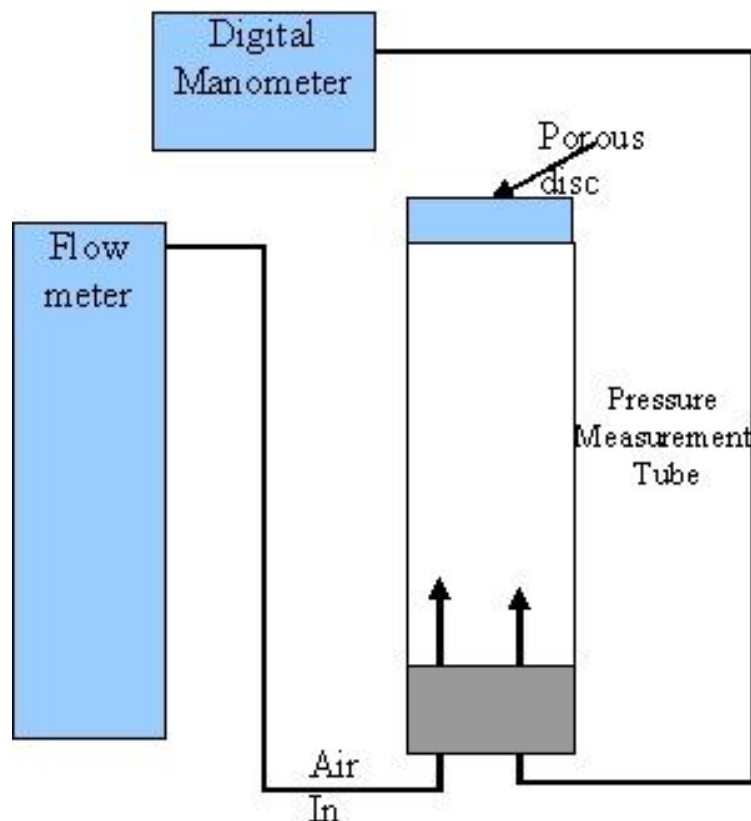


Figure 33. Diagram of Combustion Plate Experimental Apparatus

The results of the testing are displayed in **Figure 34**. The data show that the ZAL-45 is the best candidate when evaluated for this criteria.

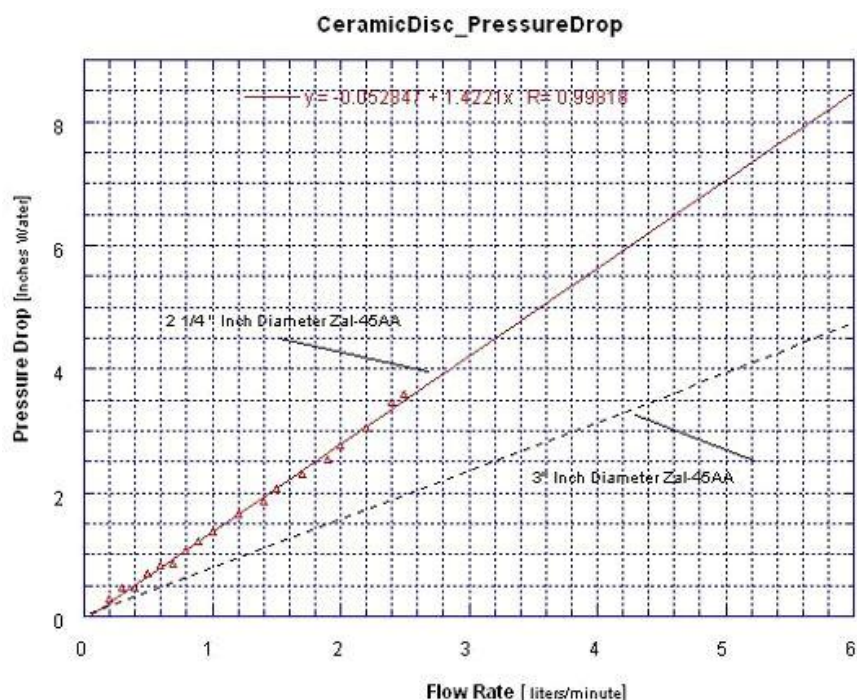


Figure 34. Pressure Drop versus Plate Parameters

All three samples provided back-pressures that were less than 1" of water, with sample thicknesses that are about twice the envisioned thickness. However the back-pressure will be considerably higher when the discs are at 600 °C. The correction factor is equal to the ratio of the kinematic viscosity for air at 600 °C to that of air at room temperature:

$$Correction = 9.8 \cdot 10^{-5} / 1.5 \cdot 10^{-5} = 6.5$$

It was calculated that a 3-mm thick disc of ZAL45-AA at 600 °C would produce a back-pressure of 3" of water, which is comfortably less than the air pump capability.

5.2.8 Catalyst Deposition Profiles

Considerable effort was expended to explore fabrication techniques to establish a 3-dimensional, well defined catalytic coating profile throughout the body of the combustion plate.

It is considered desirable, that the exit side of the plate should have a catalytic coating but the entrance side would be either completely uncoated or perhaps provided with a minimal and spatially uniform coating. A possible advantage for coating the entrance side is to allow for an easier start-up process.

Figure 35 shows a cross-section micro-graph of the front side (exit) of the combustion plate. Various gradient profiles were generated and tested throughout the project to see if a particular advantage might be gained.

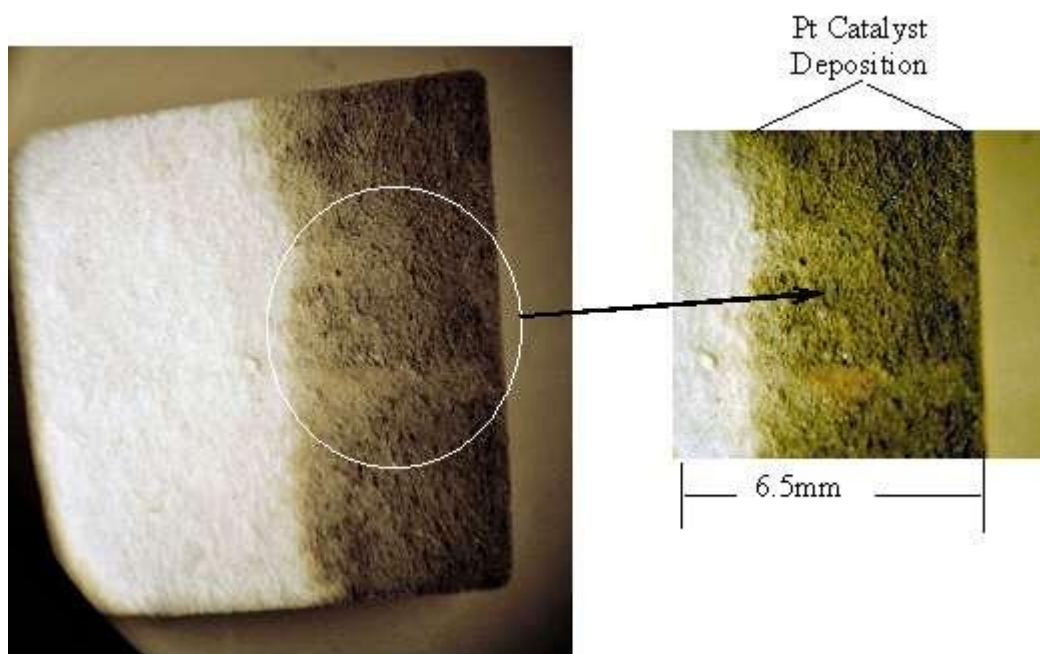


Figure 35. Catalyst Gradient Strategies for Ceramic Substrate

Varieties of methods for controlling the profile were explored. One particular approach had the property of being easy to control and reasonable in terms of labor.

The method chosen is based on a concept borrowed from the IC (integrated circuit) manufacturing industry where a diffusion blocking barrier is deposited in various places on the silicon wafer to mask off regions of silicon for doping with selected impurities.

For the porous alumina combustion plate, the issue is more 3-dimensional than normally encountered in IC manufacture where iso-planer structures are the norm.

The masking material selected for fabrication was based on a low melting, water-soluble wax that was infused into the bulk of the material at a well controlled rate (i.e., by capillary action). By stopping the capillary action at a predefined time, the depth of penetration of the wax is determined. The wax also needed to have the property that it would sublime at temperatures below its combustion point to avoid depositing carbon residue during the barrier removal stage.

After the wax solidified in spatially well defined bulk regions of the disk, the disk is then infused with the catalyst pre-cursor solution and allow to dry. It is then placed in an inert atmosphere and heated slowly to 600 °C. During this time, the wax turns into a gas and leaves the porous disk with any residue, after which the disk is allowed to be exposed to the ambient atmosphere to complete the reduction of the catalyst solution. The porous disk is then ready for final dimensioning (i.e., thickness, diameter, etc.) and coupling with the electric starting assembly.

Testing of the both the resultant catalyst combustion behavior and the flow uniformity (or non-uniformity) of the fuel/air stream in the porous disc was performed in an apparatus shown in **Figure 36**. A pattern of catalytically active regions are deposited across the exit face of the plate and the resulting combustion temperature was measured at each zone.

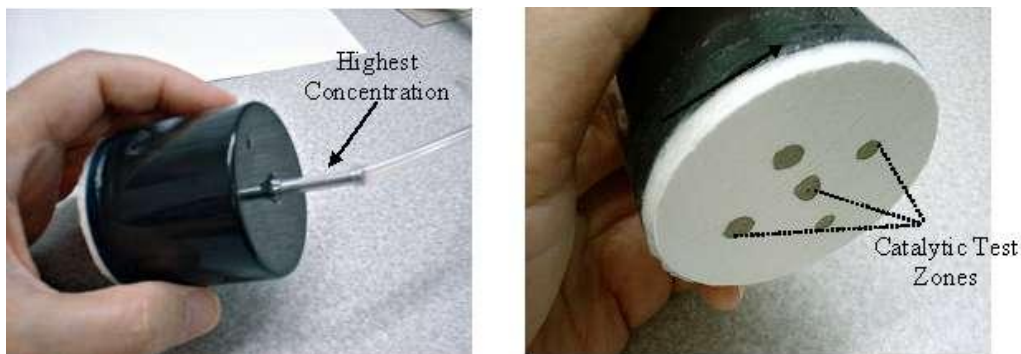


Figure 36. View of Flow Uniformity Test Cell

The fuel/air flow rate was set to 1.5 liters per minute and the total chemical power in the fuel/air stream was set to 100 watts. The flameless combustion temperatures measured at the test zones were purposely kept low so as not to allow the substantially higher viscosity of 600 °C air from altering the flow stream between the test zones.

Table 3 shows that the fuel-air was essentially distributed evenly over the surface. This can be attributed in part to the high degree of material uniformity (i.e., density and pore size) throughout the ZAL45-AA. It also shows that the fabrication process does not leave behind residue that may affect the flow stream adversely.

Table 3. Fuel/Air Uniformity Experimental Results

	Center	Top Left	Top Right	Bottom Left	Bottom Right
Temperature	500°F	490°F	510°F	505°F	495°F
Flow Rate	1.5 l/min	1.5 l/min	1.5 l/min	1.5 l/min	1.5l/min
Total Fuel-Air Energy	100 watts	100 watts	100 watts	100 watts	100 watts

5.2.9 Improved Catalytic Combustion Plate Properties

The combustor plate designs from earlier in the project consisted of either a porous ceramic material (e.g., ZAL-45A) or a refractory felt material, each coated with ample amounts of activated platinum.

The porous ceramic plate had issues with a relatively slow light-off, whereby the central region was started first and the reaction spread slowly out toward the periphery of the disc. This could take several minutes to achieve equilibrium condition.

It was speculated that the relatively large thermal mass of the ceramic extended the time to thermal equilibrium.

To address this issue, the porous ceramic was replaced with a simple refractory felt (silica-alumina) material. This reduced the thermal mass and allowed for a quicker light off and thermal equilibrium; however, a condition of fuel condensate dripping from the sides of the combustor plate was experienced after a period of unit operation. That is, it appeared that a portion of the fuel droplet stream from the nebulizer was precipitating out as a liquid and passing through the combustor plate in an un-reacted condition.

To solve these two issues and additionally improve robustness of the catalytic plate, a study was undertaken to review possible alternative materials. The material would need to have a very low density, withstand refractory type temperatures, have good thermal properties, be easy to fabricate and have the ability to tolerate mechanical abuse without being seriously damaged. One such candidate, a low density refractory metal foam, appeared to meet these requirements.

To appreciate why the thermal characteristics of metal foam improve combustor plate performance, it is necessary to examine both the macro and micro properties of the foam metal.

Figure 37 summarizes some important equations that influence both transient and steady state thermal behavior. Equation 1 describes the relationship between thermal diffusivity and the intrinsic properties of any material. Equation 2 describes the Wiedemann-Franz law.

Equation 1: $\alpha = K / (\rho \times C_p)$

where : α = thermal diffusivity
 K = thermal conductivity
 ρ = density
 C_p = specific heat capacity

The Wiedemann-Franz law states the relationship between temperature and thermal and electrical conductivities

Equation 2: $\frac{K}{\sigma} = LT$

Or $K = \sigma \times L \times T$

Where L = Lorenz constant
 σ = electrical conductivity

Figure 37. Relationship Between Thermal & Electrical Conductivity

P. Grootenhuis, et al reported on the relationship between thermal and electrical properties of porous metals (i.e., metal foam) in 1952 Proc. Phys. Soc. B 65 502-511. It was determined that to a first order approximation, electrical conductivity was independent of particle size but correlated well with density and, in addition, were in a linear relationship with density. Using the Wiedemann-Franz law to connect the thermal conductivity, we see that thermal conductivity is also linear with density.

Figure 38 shows a microscopic comparison of a refractory metal foam consisting of 100 ppi (pores per inch) material placed next to an 80 ppi material. Physically, 100 ppi material is very similar to the 80 ppi material on a substructure level, but the nodes are smaller and closer together. This may have an effect at higher temperature where the nodes are "communicating" through radiative heat transfer. The foam is processed so that the active sites tend to be largely on the nodes.

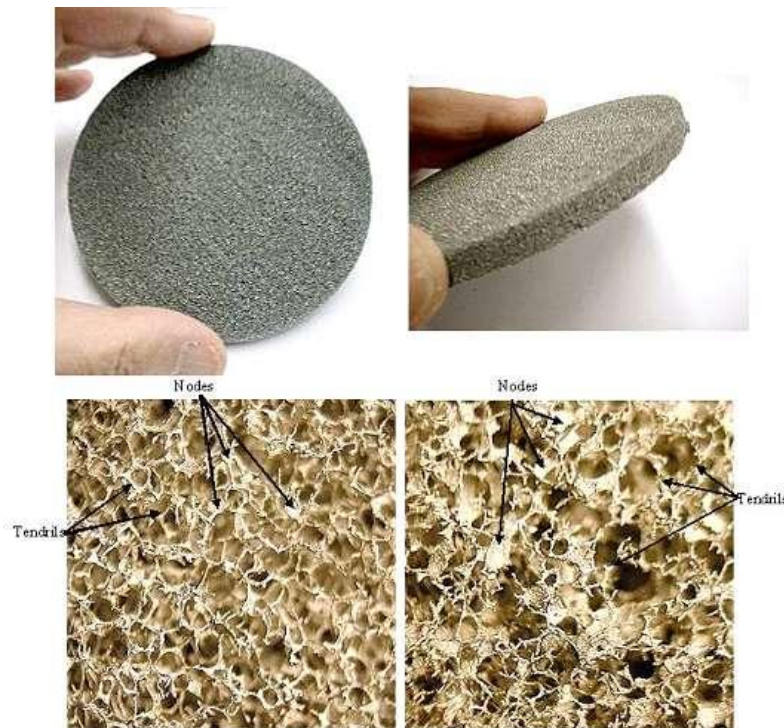


Figure 38. Metal Foam Combustor Plate Physical Structure

Based on this macro level view of the metal foam, the density and the thermal conductivity appear to be changing to the same degree and in the same direction. Surprisingly, this predicts, that the thermal diffusivity is roughly the same for the foamed metal as in the bulk metal (i.e., non-porous material). This is because the specific heat factor in the equations do not change when calculating bulk level parameters, it is tied to the mass; thus, the micro and macro values are the same. This implies that the temperature gradient between the two surfaces of the combustor plate would be relatively small (i.e., assuming that catalyst is applied uniformly throughout the metal foam) even though the micro-thermal conductivity is very low.

Attempts at measuring pressure drop across the metal foam at room temperature showed that the flow impedance was immeasurable using the standard digital monometer used for earlier tests with the porous ceramic materials. Typically, the tubing that connects the monometer to the test set-up contributes negligible amounts to the recorded value. However, the metal-foam porosity is so high that its pressure drop contribution is overwhelmed by the connection to the test apparatus; therefore, it can be estimated that, at an air flow rate of 6 liters/minute, the contribution of the metal foam plate to pressure drop is less than 0.05 inches of water. This opens up a whole new regime of possible air moving devices that are more efficient and much smaller than the radial vane air pump that has been designed into the current model of IWH. (See, for instance, Section 5.2.2 and Figure 29).

On a micro level, the thermal conductivity, as viewed from the many thousands of metal nodes (again referring to Figure 38) is much less than bulk metal properties, because the heat must flow through slender tendrils in order to reach the next node. Thus, the thermal diffusivity at this level of dimension appears very low (i.e., node-to-node transmission). In the case of the metal foam used in this project, the densities are about 2% or 3% of the bulk stainless steel metal, so the thermal diffusivity may be presumed to be about 40 times less than the bulk metal.

Since diffusivity governs the rate at which heat energy flows away from the source of heat (i.e., catalytic reaction site attached to node), each node can be expected to be much higher in temperature than the average bulk temperature. This explains why the light-off was found to be significantly quicker. Temperature uniformity is better and droplets of fuel are impeded from getting through the matrix because they eventually impact the extremely hot ($>900\text{ }^{\circ}\text{C}$) nodes along the way, causing instantaneous evaporation.

Figure 39 and **Figure 40** show data reported by Jörg Sauerhering of the Institute of Technical Thermodynamics, in Cologne Germany. These data shed more light on the behavior of porous metal materials. In his measurements, he defines a primary porosity as the complement of the ratio between the overall foam density and the density of the microscopic tendrils (i.e., matrix).

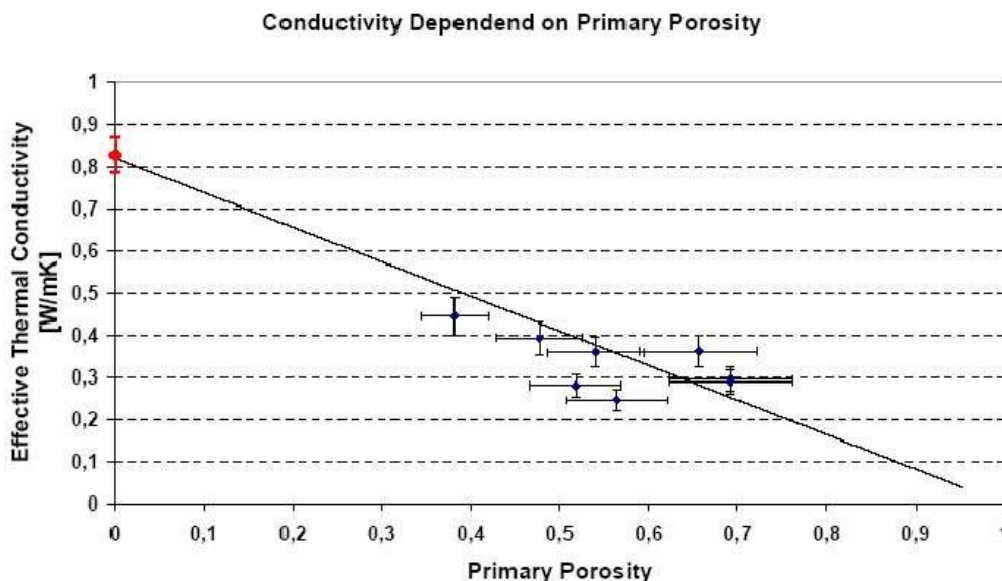


Figure 39. Thermal Conductivity vs. Primary Porosity of Combustor Plate
(note that Primary Porosity is unitless)

This particular approach to defining porosity is used because in some types of metal foams, depending on the fabrication method, the density of the tendrils may be less than the pure metal. For the foams used in this report, the tendrils should be about the same as the pure metal.

This data confirms the general contention that metal foam thermal conductivity is proportional to the bulk density of the foam and roughly with a slope of minus 1. It is interesting to note that this relationship is does not appear to be generally applicable to non-metals (based on some preliminary literature research). In non-metal foams (e.g., alumina) the change in density of the body has a markedly less effect on thermal conductivity. Thus, the use of ceramic foams is not expected to have the same benefits called out in this report for the metal foam.

An interesting effect from radiative heat loss occurs when the temperatures reach much higher levels as would be found during actual operation (i.e., catalytic combustion). Figure 40 shows how radiative transfer between the nodes can increase the effective thermal conductivity by a factor of 2 or 3.

Thermal Conductivity: Dependency on Temperature, Matrix

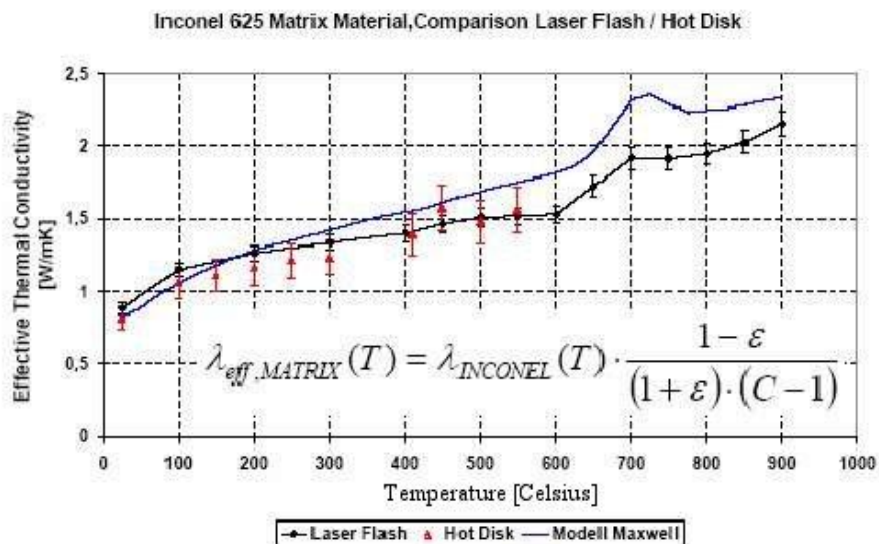


Figure 40. Thermal Conductivity vs. Temperature of Combustor Plate

This effect results in a certain degree of self regulation of the metal node temperatures, and thus increases the range of power densities that the foam can take before the metal succumbs to over temperature effects.

Although the thermal properties of the metal foam appear beneficial, the question still remained as to whether it had the necessary mechanical properties. The answer was found to be that it was far superior to previous materials in terms of mechanical properties. For instance, in actual operation the combustor plate had to be sized precisely and fit into a predetermined orifice opening in the mixer chamber. This means that the ability to make minute adjustments to the fit is beneficial. Metal foam appears to be easily adjusted without a general release of detritus, or unraveling of the fabric (i.e., as may occur in felts) or a chipping of edges as in porous ceramics.

Also, when fitting the foam to final position within the mixing chamber, a seal/gasket like component is generally pressed over its periphery to finalize the fit and keep it in position. The foam resiliency (i.e., compressibility) allows the seal to be tightened without fear of fracturing the material and allows rapid expansion during heat-up without failure of the sealing surface. In addition, the metal foams can withstand very large thermal and mechanical shocks, which occur in the normal operation of the system, without degrading performance.

5.2.10 Catalytic Starter

In this section calculation results and empirical physical designs for an electro-catalytic starter (ECS) are explored.

A critical system element in the successful operation of the catalytic IWH is the mechanism for starting the catalytic reaction. While it is common in some types of catalytic combustors to provide an open flame, this was not considered an option for the design parameters of the current application.

Electrical energy, controlled by an embedded intelligence, is the preferred approach since it is safer and allows automatic starting. However, because electrical energy for portable application depends on batteries, optimization of the starting mechanism, to reduce energy requirements is necessary to keep batteries small and light weight and to increase the number of starts between battery changes.

In the future, the use of TEG devices may be used to charge the battery during use to eliminate changing the battery during the useful lifetime of the IWH unit.

The physical principles underlying the ECS are joule heating and catalytic light-off. Conceptually, the scheme is to first provide ohmic heating to a region located in the path of the fuel/air stream, just above the main catalytic plate combustor, and then allow the generated heat to raise the temperature of a small mass of catalytically active material, causing a catalytic light-off of the fuel/air mixture and a consequent propagation of the catalytic reaction front throughout the combustion plate.

Use was made of the CFD modeling package known as Cosmos FlowWorks. This CFD package is a moderately sophisticated tool for simulating real world fluid mechanical and heat transfer problems. Empirical data was also obtained and used to confirm the model results.

The first step in the process was to reduce the model to the most basic physical representation of the real device and examine the details of the ignition process. The fuel/air stream is assumed to be directed normal to the catalytic combustion plate and have sufficient air present to complete combustion if it were to start. It is not economically feasible to provide a starting condition over the whole combustion plate surface, so it becomes important to direct the effort toward optimizing a design that allows localized starting to propagate across the combustion plate surface.

When the droplets arrive at the plates inner surface, they immediately begin to be absorbed by the porous structure and if not quickly reacted, could lead to a "wet-out" condition where the plate is over-saturated with unburned fuel, thus preventing catalytic action from beginning. The starter, therefore, must be very quick in its light-off process to prevent this condition. This leads to the conclusion that the transient as well as the steady state (i.e., equilibrium temperature) starter temperatures are import criteria.

Both of these values are calculated for a range of starting powers. For this study, the starting parameters were between 5.55–10 watts. This range of power was chosen for practical reasons having to do with portability of the end application and the need for readily available battery chemistries. Thus, the energy requirement to achieve starting temperatures needs to be minimized in order to allow small and lightweight batteries. This in turn points to the need for the starter to have low thermal mass.

In summary, the following system requirements were used to guide the design approach:

- The need for a rapid climb to light-off temperature
- Minimize the light-off temperature
- Assure that droplet coalescence is minimized

The third condition directs the design effort to pay special attention to the surface temperatures to which the droplets come in contact. To assure that the droplets do not merge into a larger mass at the surface of the starter, and to prevent the accumulation of residue on the starter materials, the starter should quickly reach a temperature above the boiling point of the majority of the hydrocarbon components contained within the fuel.

This condition can be met by assuring that the average temperature of all contacted surfaces reach 500 °C or more in a time period shorter than the agglomeration rate of fuel droplets. As we see from **Table 4**, at the 500 °C temperature greater than 95% of the components of most kerosenes will vaporize. If this happens rapidly enough, it will prevent build up of fuel droplets into a single larger mass.

The first condition drives the design toward the use of low thermal mass for the starter components and the proper degree of thermal isolation from the combustor plate.

Table 4. Fuel Temperature vs Fractional Boiling

Temperature vs Evaporation Results	Kerosene CAS# 8008-20-6	Kerosene CAS# 64742-81-0
Initial Boiling Point	238 °C	362 °C
10% Components Evaporated	327 °C	392 °C
50% Components Evaporated	405 °C	434 °C
90% Components Evaporated	475 °C	488 °C
95% Components Evaporated	490 °C	506 °C

The second condition drives the design toward having two types of catalytically active structures within a single igniter assembly. The first catalytic structure is realized by combining the joule heating function of the filament with a catalytically active ceramic coating. The filament is coated with a high surface area (i.e., micro level) ceramic alumina, which is then infused with a platinum catalyst solution. Since the catalytically active ceramic coating is in direct contact with the filament, it reaches the filament temperature almost simultaneously.

Figure 41 shows an actual assembled and working igniter device. Its overall dimensions are 0.800 inch wide by 1.157 inch long for an overall projected area of about 0.9256 square inches.

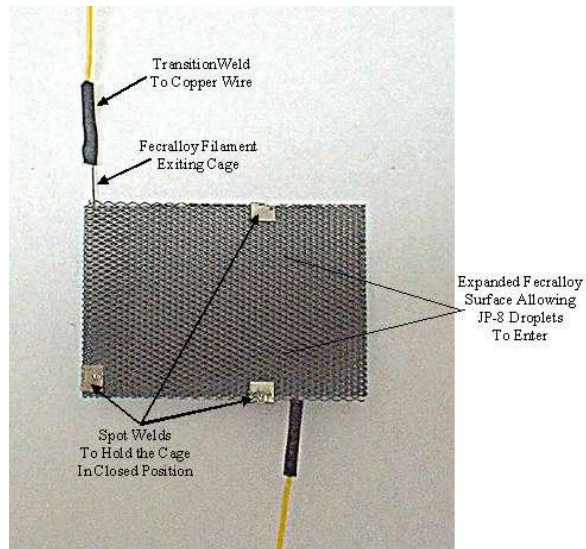


Figure 41. Top View of Assembled Catalytic Starter Device

The filament is formed into a simple serpentine pattern in order to fit within confines of the cage screen shown. **Figure 42** shows the catalytically active filament just before it is formed into a serpentine pattern.

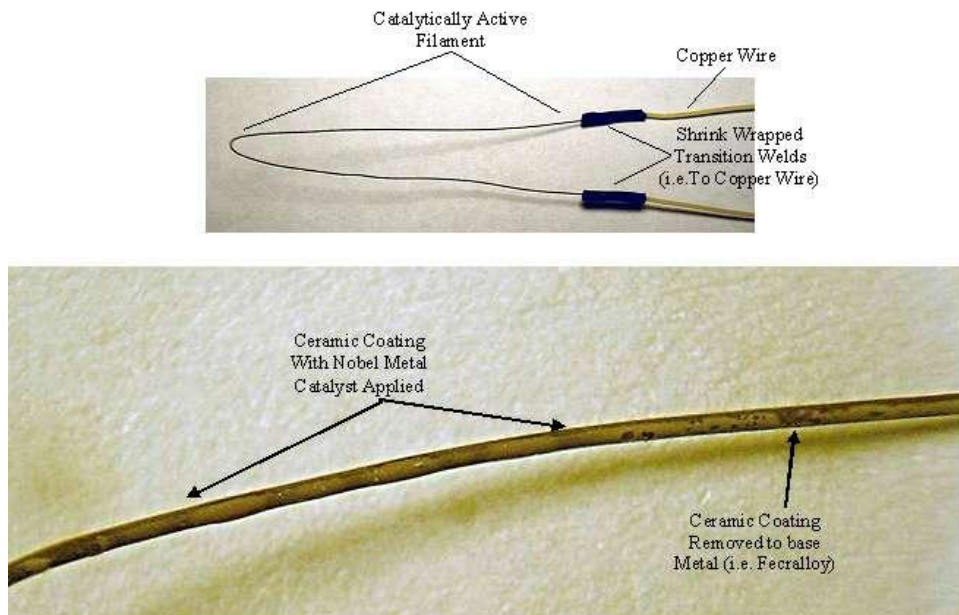


Figure 42. Close-up View of Ceramic Coated Filament w/Catalyst Applied

The upper portion of Figure 42 shows the basic physical structure of the filament. The filament starts as a Kanthal A-1, 3-mil-diameter wire. The length of the wire is chosen to allow at least 4.5 ohms of resistance. This is obtained with about 4 inches of wire length.

The wire is then heat treated to allow a layer of oxide to appear. The wire is then coated in slurry of alumina particles and heat treated again to form a ceramic layer. The ceramic is then

converted to gamma alumina to increase the microscopic surface. At this point is ready to be coated with the noble metal catalyst.

The bottom portion of Figure 42 shows a close up view of the ceramic coating attached to the oxidized wire core.

The next step is to provide a connection to the "outside world" of copper wire by cleaning the ends (i.e., removing the oxide) of the wire and micro-welding 30 gauge copper wire to each end. At this point the welds are protected with shrink wrap. The filament is then positioned onto an unfolded portion of the cage screen and topped with a gossamer-like layer of catalyst coated, alumina micro-fibers. **Figure 43** shows the cage screen before the filament is inserted. Note that although the filament is in direct contact with the cage screen it is electrically insulated by virtue of the oxidized coating and the baked on ceramic layer. Also, the cage screen itself is oxidized to further electrically isolate the two components.

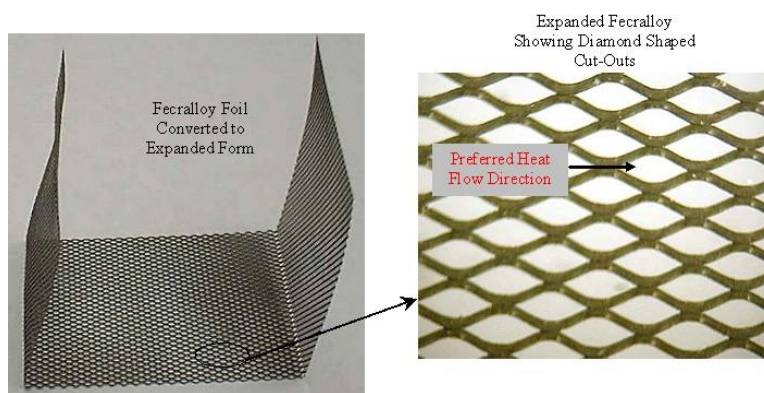


Figure 43. Catalytic Starter Cage Close-up

The purpose of the cage screen component is four-fold:

- To support and align the catalytic fibrous alumina mat with the catalytically active joule heating filament.
- To thermally isolate (mildly) the active igniter components (e.g., filament & alumina mat) from direct contact with the combustor plate.
- To provide physical support and mechanical integrity to the whole assembly.
- To act as a collector of the fuel droplets by intercepting and holding onto (i.e., by capillary action) them using the intrinsic surface properties of the diamond shaped pores (i.e., screen openings).

To further insure a quick light-off, a second catalytically active component that has a relatively large projected area (i.e., larger than the filaments projected area) is required. The large planar surface area of this ultra low density catalytic structure is placed directly over the electrically heated filament.

To fulfill this requirement, a planar mat of ultra low density micro alumina fibers were coated with a noble metal catalyst. An example of these catalytically-coated micro fibers is shown below in **Figure 44**. The left portion of the figure shows a microscopic view of the pure alumina before it has absorbed the noble metal catalyst. The fibers are about 5 to 10 microns in diameter.



Figure 44. Microscopic View of Catalytic Starter “Light-Off” Promoter

This particular alumina material is so low in density that it is very fragile. Without the cage to protect it, it would fall apart with ordinary handling. The low density is an advantage, however, when it comes to enhancing the light-off properties of the catalyst.

Because of its low average density, the electrical filament heat energy raises the outer surface temperature of the micro fibers to an incandescent radiant state, causing a chain reaction throughout the mat (i.e., as long as there is enough local fuel/air supply). This is somewhat analogous to the way tinder is used to start a normal flame combustion fire. Because each fiber has extremely low thermal mass, only minute amounts of energy are required to bring the micro fibers to a high temperature nearly instantly.

To investigate the peak temperature that might occur during the igniter start-up sequence, it is necessary to plot the surface temperatures over the surfaces of both the filament and the cage screen structure. CFD calculations were done for both the steady state and the transient conditions.

Only the transient calculations are shown here. The transient plots capture both the peak temperatures and the time necessary to reach these values. This impacts the choice of battery chemistry to assure a long battery life. **Figure 45** shows the time dependent calculation for a 5-volt pulse driving the starter assembly. This is equivalent to an electrical power of 5.5 watts.

The steady state surface plots (not shown) indicate that portions of the filaments surface do reach T_C , even though in Figure 45, the integrated average temperature does not. The cage screen however, does not show any portion of the surface reaching the critical temperature. The transient plots indicate that in a two-second period, even the filament falls below this critical temperature.

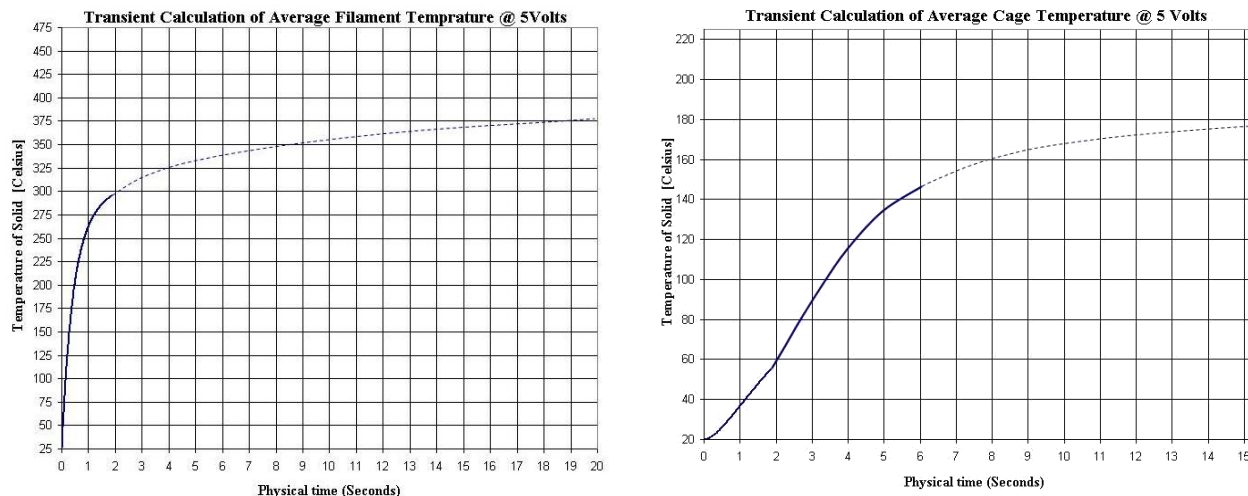


Figure 45. Transient Temperature Calculations for 5 Volts

Figure 46 shows the time dependent calculation for the case where the starting pulse was increased to a 10-volt level. This is equivalent to an electrical power of 22 watts

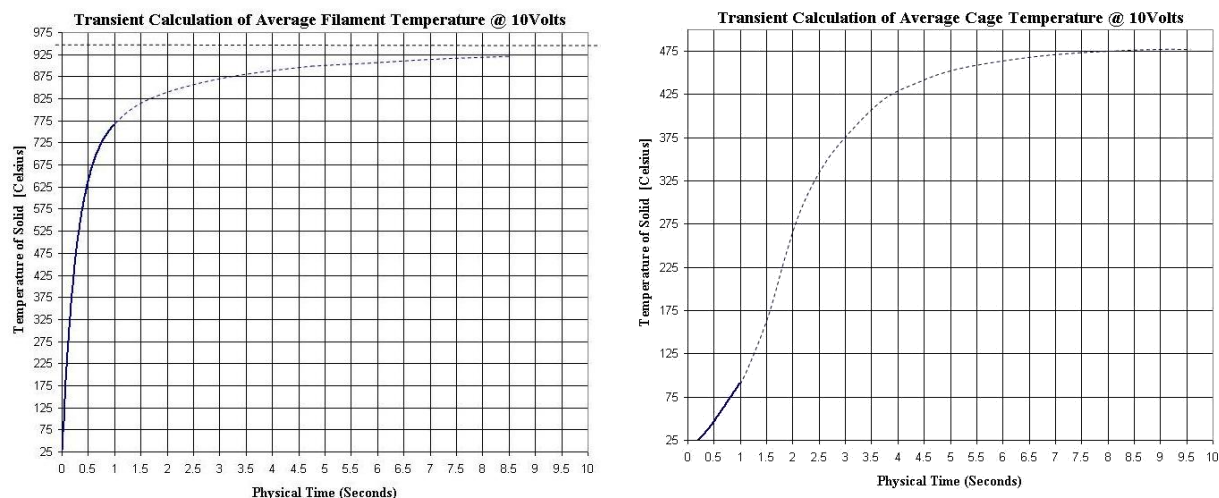


Figure 46. Transient Temperature Calculations for 10 Volts

The steady-state surface temperature plots (not shown) for a 10-volt source show that the filament will just about reach the thermal limit of the cage material (i.e., 1050 °C) if left on for an extended period (10 of seconds). Realistically, the power required to do this is not something that would ordinarily be available from a small lightweight battery.

Actual system performance data shows that an intermediate voltage value (6.5–9.5 watts), applied for about 5 to 10 seconds, would work well for all anticipated circumstances. This is because once the catalytically active filament and promoter light-off, the extra energy from the catalytic heat reaction will quickly add to the battery supplied energy, causing all the surface temperatures to successfully reach the flameless ignition point.

The small 123 type lithium battery is an example of a battery type that could perform this function if limited to a couple of seconds and very low duty cycle (i.e., starting the unit a few times per day).

Future igniter designs might focus on further optimizing the igniter to allow even less power for a reliable light-off.

Prototype testing was performed by system integrator Creare, Inc. to measure performance of the catalytic pass-through water heater using JP-8 as the fuel. To provide a rational guide for improving the performance of the device, based on the input from Creare, CDI developed a computer model.

A series of eleven modeling experiments were performed requiring about 100 hours of computer time and several days set-up time per model, to establish design criteria for each of the eleven models. **Figure 47** shows the CFD experimental design.

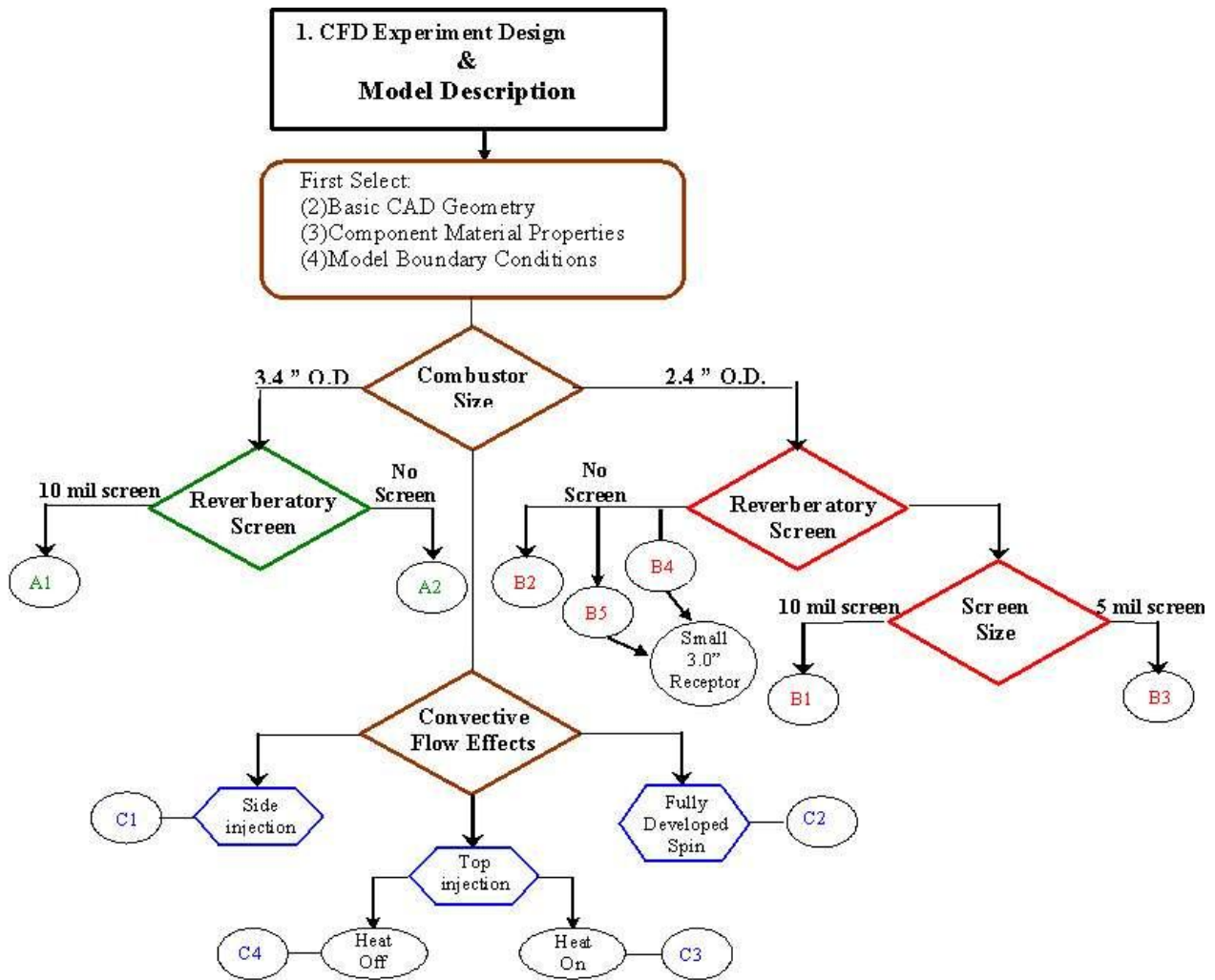


Figure 47. Flow Chart Showing Areas of Potential Heat Transfer Improvements

The goal in this study was to perform an array of "what if" scenarios where specific features of the design are modified based on either first principles or scientific intuition and then to calculate the result to see if the scientific intuition is justified.

The results of this modeling provided recommendations to modifying the current design in order to achieve improved performance. The recommendations primarily addressed the following three issues:

- What can be done to eliminate unburned fuel "pass-through" condition?
- What can be done to increase overall device heat transfer efficiency to the water?
- What can be done to reduce weight and size of the unit?

The first step in the process is to select the basic CAD geometry, component materials and boundary conditions that best represent the real world conditions of the current device.

Figure 48, shows the basic CAD geometry and calls out the boundary conditions used throughout most of the experiment.

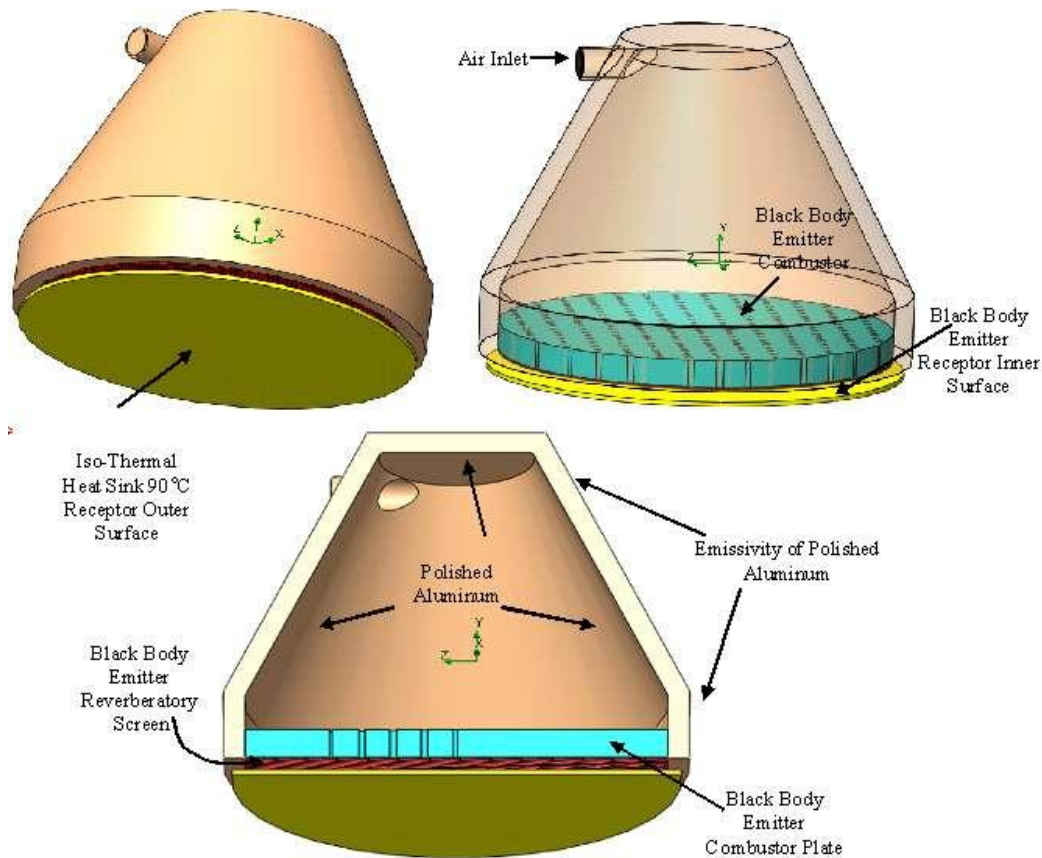


Figure 48. Illustration of CAD Model Used in CFD Study

In particular, the four basic components of the model consist of:

- (a) The mixing chamber; which is made from aluminum and has a radiant emissivity of polished aluminum for both the interior and exterior. The only exception to this is in experiments B4 and B5 where the interior emissivity is changed to a black body -- with dramatic results.
- (b) The receptor plate; which is aluminum and had the bottom side set with a boundary condition that simulates a water heat sink set to 90 °C and a top side (facing combustor plate) that is a black body surface.
- (c) The combustor plate; which is made from an insulating like material that simulates the porous ceramic properties. It has radiant surfaces that are black body in nature.
- (d) The reverberatory screen, that is made from stainless steel and was modeled in two basic configurations, one that has a 10 mil wire diameter and 10 mil spacing and the second which has a 5 mil wire diameter and a 15 mil spacing.

Each of the eleven model scenarios included heat losses from radiation, convection, and conduction.

In all of the CFD experiments, the effects of both radiant emission/absorption of surfaces and convective effects were included so that real world heat transfer would be simulated as close as possible. This tended to make calculation-times per modeling-run on the order of 4 to 8 hours depending on the coarseness the finite element mesh generation.

Initially, several runs were performed without convective effects (i.e., no gravity) to see the degree of influence on the end result. It was determined from this (and first principles) that convective effects and turbulence were significant and should be included in the calculation.

Figure 49 shows a close up view of the reverberatory screen geometry used in the model. The material is specified as being stainless in the model. In theory, the reverberatory screen functions primarily by picking up heat from the hot gasses exiting from the combustor plate and by absorbing the radiant energy from the combustor plate surface. This extra heat is trapped between the grid and the combustor plate, causing the exit surface of the combustor plate to reach higher temperatures than if the screen were not present. As a result, the overall efficiency of the system increases.

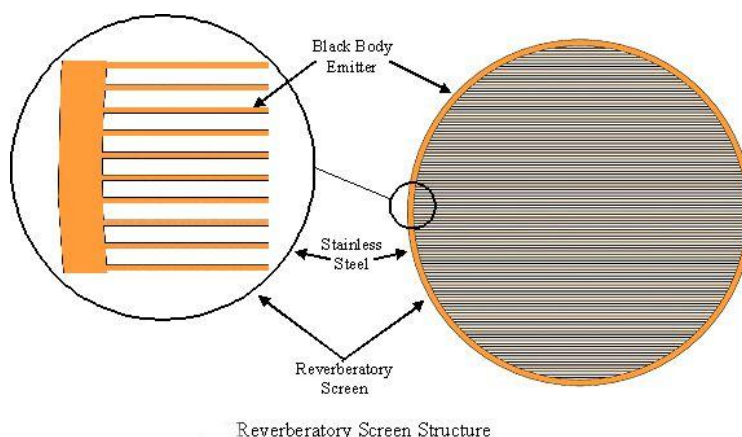


Figure 49. Reverberatory Screen Effect on Radiative Heat Transfer

For calculation purposes, the reverberatory screen is placed within 10 mils of the combustor plate surface. The screen's wire grids (very low mass) tend to quickly reach temperature levels approaching or even exceeding the combustor plate exit surface temperature because of their low mass. All calculations with the screen were done by setting the screens surface emissivity to be a black body type.

The combustor-plate CAD model was chosen to be 6 mm in thickness and designed with enough pores structures built into the plate to insure a very minimal pressure drop for a 6 liter per minute flow rate (with the power turned off). This was necessary to simplify the model and reduce calculation times. Pressure drops in the model were calculated to be 10-20 pascals, rising to 50-60 pascals at steady-state powered-up condition. This is one of the few differences between known real life model characteristics and the CFD model.

The choice of such a minimal pressure drop design should not appreciably change the relevance of the data obtained, since flow rates, surface temperatures, convective and radiative heat transfer are the primary determining factors in the steady state profiles.

Actual laboratory data show pressure drops during operation that are on the order of 100 Pa. This is not too much higher than the model selection. However, this is still very low (i.e., 0.5 inches of water pressure), with the resulting effect on fluid viscosity, stored energy (in the air) and air flow patterns likely to be negligible. Thus, the model is felt to be “trustworthy”.

The calculation shows that the use of a smaller combustor plate in the model achieves plate temperatures that are at least 200 °C higher than the larger 3.0" diameter combustor plate used in the early prototypes, even though the total energy generated by catalysis (350 watts) and the flow rates (6 liters per minute) are exactly the same in both models. The principal reason for this is that a higher power density is obtained in the smaller combustor plate.

An important concern with the current table top demo version has to do with fuel not completing combustion and passing through the combustor plate into the environment and re-condensing as droplets.

Temperature profiles were compared across the large plate and the smaller 2.4" O.D. plate. One feature that was clearly revealed on the larger plate, is a rapid drop in plate temperature, starting at about 1 cm from the mixing chamber wall. The smaller plate still retains a reasonable temperature near the wall of the chamber (about 500 °C) as compared to the much lower 350 °C temperature of the large plate. This suggests a possible scenario where the outer edges of the larger combustor plate are simply not reaching the critical value needed to insure complete combustion. This result supports the idea of using a smaller plate size with its higher combustion temperatures.

Of course, reducing the combustor plate size increases the surface temperatures of the surrounding mixing chamber with the potential for increased convective and radiative losses and thus might, at first consideration, counter the benefits of this approach. This was examined further and was found to not be an important issue according to model calculations.

The net energy absorbed by the receptor plate (i.e., heat exchanger) is the ultimate judge of the effects of any design change on the efficiency of the device. That is because the receptor represents the part of the model where all the heat is intended to be transferred (i.e., for the purpose of heating water).

The top surface of the receptor is placed within 0.1 inches of the mixing chamber exit rim. All the experiments except B4 and B5 were carried out with a receptor size of 3.6" O.D. The experiment B4 was with a receptor O.D of 2.6". Experiment B5 was the same as B4, but with the receptor edge made into a 1"-high lip to help recuperate some of the exhaust gasses. Results showed that the receptor was able to receive about 60% of the energy generated in the combustor plate (i.e., 60% of 350 watts).

The top image in **Figure 50** shows the fluid (air) temperature and flow patterns in and around the top of the receptor plate. The top portion of the receptor plate is where all of the heat energy is transferred to the water flowing in the heat exchanger.

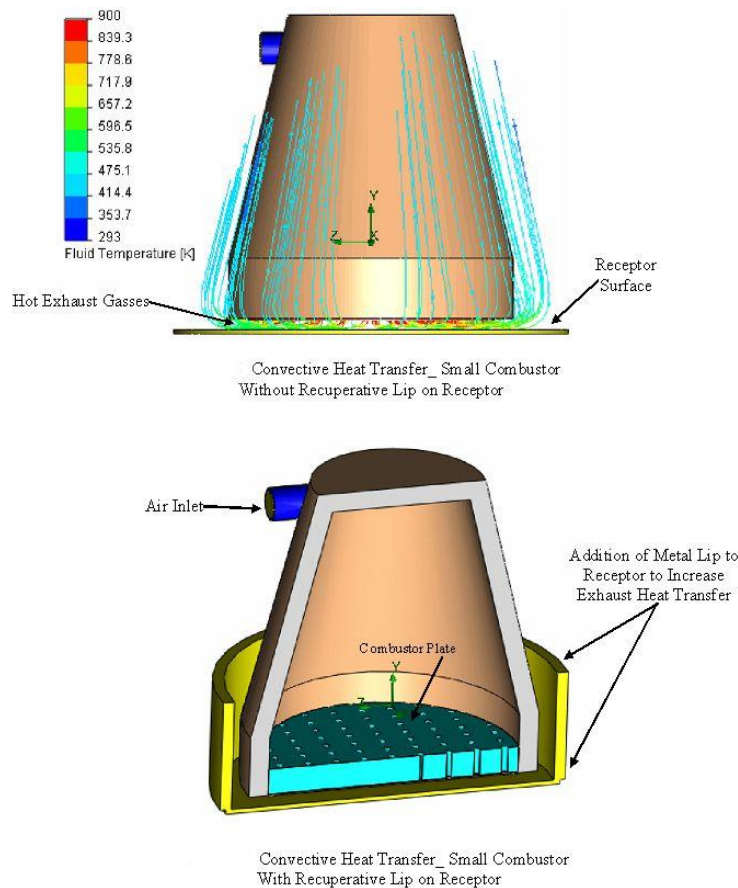


Figure 50. Recuperative Heat Design Change

The simplest way to model this is to set the bottom of the receptor plate at a fixed temperature (90 °C). In this way, the CFD model treats the receptor bottom as an infinite heat sink, absorbing as much energy as the combustor puts out. Since the actual device is under the control of a feedback-loop to maintain the water temperature (by increasing or decreasing the water flow rate) at a constant value, this boundary condition closely resembles reality.

The bottom image in Figure 50 shows the model being altered to determine if it is worthwhile to increase the path length over which the hot exhaust gasses travel before being expelled into the atmosphere. In principal, this should increase the efficiency of the system by recovering the energy in the hot exhaust exiting from the combustor plate. Model results indicate that an extra 10 percentage points in efficiency is achieved when the lip is added.

Figure 48 showed a set of experiments labeled C2, C3 and C4. These are respectively:

- (a) A condition where the air enters the top of the mixing chamber with fully developed spin;
- (b) Air enters the top of the chamber with no spin but is fully developed; and
- (c) Air enters the top of the chamber but the heat is turned off to examine the effect on the flow patterns.

The top and bottom portions of **Figure 51** show the effect on air flow patterns. The resulting patterns are typical of conditions where the buoyant forces (i.e., convection) are well in excess of the inertial forces (i.e., stream velocity). The patterns shown are for the large combustor plate configuration and so the stream velocity is very low for the 6 liters per minute air flow input rate.

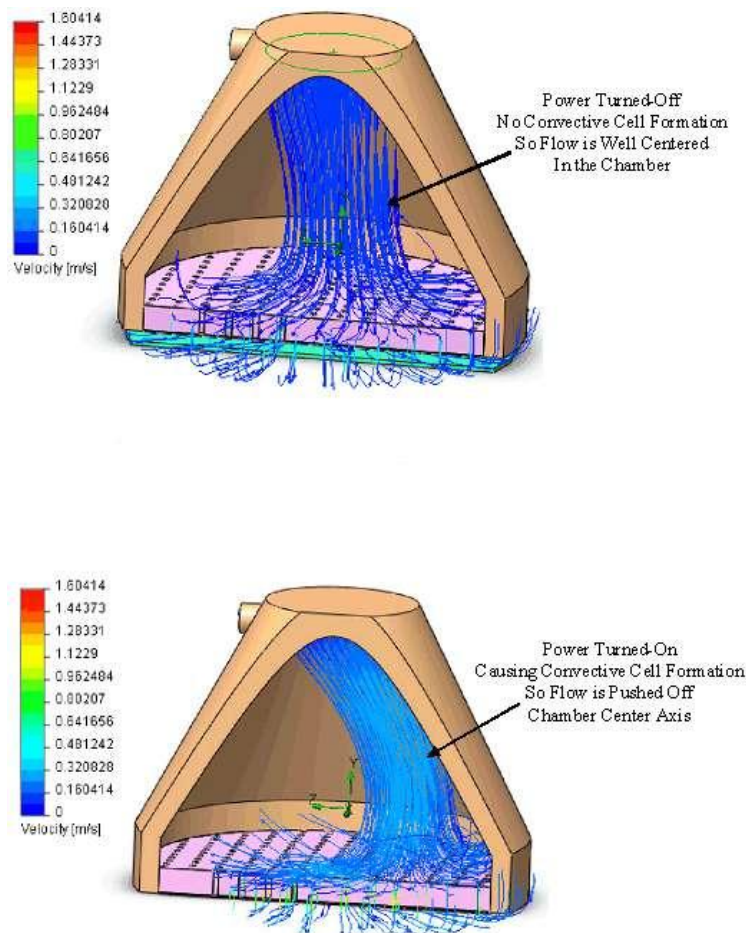


Figure 51. Illustrated Effect of Internal Convective Cell Formation on Fuel Delivery

By switching to a smaller combustor plate the resulting stream flow velocity increases and consequently a slightly more centered flow pattern occurs. However, the pattern is still quite significantly perturbed.

To help insure that the fuel droplets being emitted from the nebulizer are uniformly distributed by the time they reach the combustor plate, the prototype was designed with an air inlet stream forced to develop a swirl-like flow pattern as it entered the combustion chamber.

In the top portion of **Figure 52**, this particular flow injection condition was investigated by mathematical modeling. In the actual prototype, it is unlikely that the swirl pattern is completely developed before it intercepts the nebulizer droplet stream.

To see if this would in any way adversely affect the convective cell formation, the model shown in Figure 52 was given a boundary condition that forced a fully developed swirl. The result

showed that non-uniform flow patterns appear regardless of whether the swirl is fully developed or not.

However, in the bottom portion of Figure 52, we see the result of a very simple change, whereby the interior of the mixing chamber is painted black to force a black body type radiative boundary condition. In doing this, the gas convection cells were smaller and, perhaps more importantly, arranged in a symmetrical pattern around the central axis of the mixing chamber. So it appears that if the interior is coated with a high-temperature black paint, the flow stream maintains a central axis orientation.

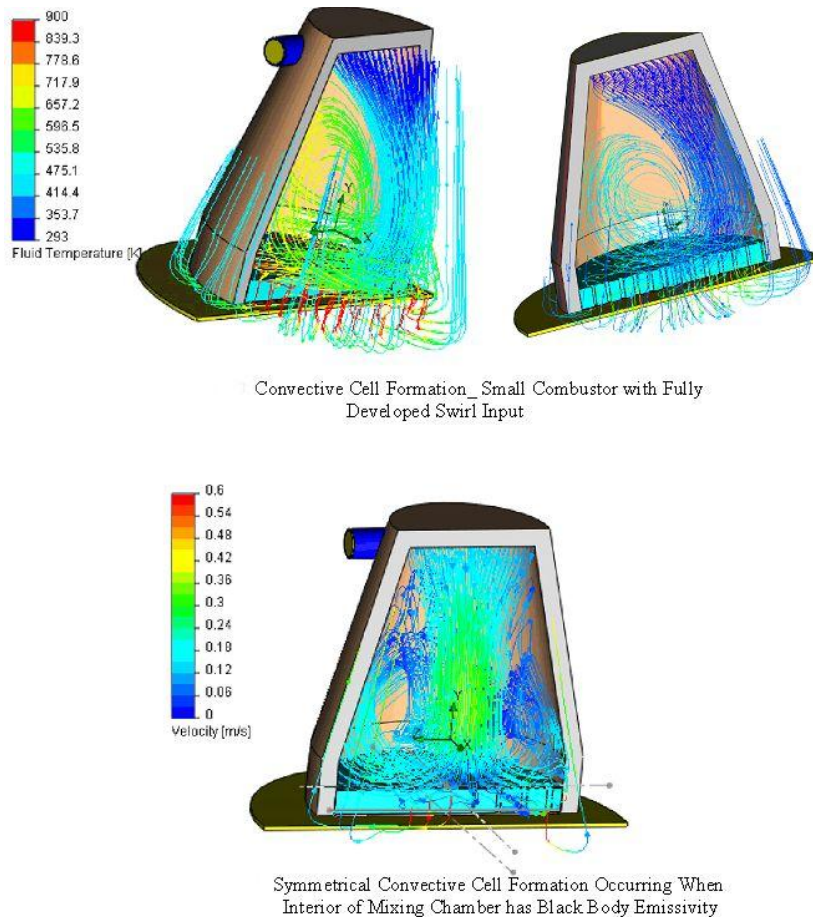


Figure 52. Convective Cell Formation with Fully Developed Air Swirl Input

The importance of this is that the fuel droplets will then be directed more uniformly across the plate. It not known at this time whether the axial off-set of the flow pattern, predicted in these models is a significant contributing factor to the fuel leakage (i.e., unburned fuel crossing the plate) reported by Creare, but it seems prudent to suspect it was a contributing factor and eliminate it if the other concluding recommendations are not sufficient.

One potential drawback to making the interior of the mixing chamber into a blackbody radiator is that the interior temperature increases and may adversely affect the nebulizer device operation. However, it is felt that if there was an adverse effect, it could be mitigated by a variety of

approaches. It is interesting to note that the overall efficiency does not suffer (when compared to B2) as might be expected from the higher temperatures of the mixing chamber (e.g., convective heat transfer losses) probably due to a compensating effect of increased radiative heat transfer. Thus, from a purely efficiency perspective, the higher operating temperature is not a detriment.

6. Conclusions/Recommendations

Error! Not a valid bookmark self-reference. summarizes the recommendations arrived at through the use of a detailed CFD modeling study covering 11 different model variants shown Figure 47. Two of the four recommended design changes were implemented in the final prototype and provided performance improvements. The reverberatory screen and recuperative geometry were not implemented in the prototype due to lack of time.

The anomalous behavior experienced by Creare's regarding uncombusted JP-8 fuel condensate leaking from the combustor plate, after a short period of operation, was reported to have been resolved through the use of the new metal foam combustor material structure and a reduction in combustion plate diameter

Overall efficiency of heat transfer to the receptor was also improved by adapting a smaller diameter combustor plate.

It was determined that flow injection conditions such as fully-developed linear or swirl-type injection of the air into the mixing chamber appeared to have no substantial effect on the formation of asymmetrical flow patterns. These asymmetries are thought to be a contributing factor to the fuel droplets not being consumed in the catalytic process.

Independent of the fuel pass-through issue, asymmetrical flow patterns generally are undesirable because of the non-uniform heat distribution within the catalytic combustor plate. Non-uniform surface temperatures are inevitable but the magnitude of the temperature gradients are difficult to predict since the flow patterns are irregular.

The thermal properties of the porous metal combustor plate, as discussed in section 5.2.9 may have mitigated much of the expected gradients by rapidly diffusing heat build-up in any portion of the plate.

By applying all of the modifications recommended in this report it is believed that not only will the unit function at higher efficiencies, complete fuel combustion, but also be lighter and more compact.

Table 5. CFD Recommended Design Changes and Conclusions

Description	Recommend	Not Recommended	Undecided	Comments
Smaller Diameter Combustor Plate	Yes			-- Higher edge & central temperatures for combustor plate
				-- Higher Russell number (i.e., ratio of inertial to buoyant forces) causing smaller and fewer convective cells
				-- Better effect of reverberatory screen
				-- Faster starting
Addition of Catalytic Reverberatory Screen	Yes			-- Increases overall heat transfer efficiency
				-- Addition of catalyst will act as afterburner for any fuel pass-through.
Increase Emissivity of Mixing Chamber Interior			Yes	-- Counters the formation of convective cells and increase symmetry of cells
				-- The increase in internal mixing chamber temperatures that occur with this change may be a problem for the vibrating mesh operation
Receptor Plate Size Reduction and Geometry Change	Yes			-- 15 % more heat transfer from exhaust gas with one inch recuperative lip on edge of receptor
Changing Flow Injection Type		Yes		-- No substantial differences noticed in the model
Low Thermal Mass & Low Thermal Conductivity	Yes			-- This has already been implemented successfully in prototype form.

This document reports research undertaken at the U.S. Army Natick Soldier Research, Development and Engineering Center, Natick, MA, and has been assigned No. NATICK/TR- 10/018 in a series of reports approved for publication.